

A varying parameter multi-class second-order macroscopic traffic flow model for coordinated ramp metering with global and local environmental objectives

Apostolos Kotsialos

Public Power Corporation – Hellas S.A., Greece



ARTICLE INFO

Keywords:

Second order macroscopic traffic flow models
Multi-class modelling
Hot gas emissions
Ramp metering
COPERT
Differential evolution

ABSTRACT

This paper presents the design of a coordinated ramp metering strategy based on a newly developed multi-class second-order macroscopic traffic flow model coupled with a pollutant emissions model. The approach followed for obtaining the parameters of the multi-class model is based on sigmoid surfaces spanning over traffic density and composition. An optimal control problem is formulated for designing an environmentally sustainable, efficient and equitable coordinated ramp metering strategy. In addition to the global network-wide objective of total emissions minimisation, two different types of environmental constraints are introduced for addressing local requirements. The resulting static large-scale optimisation problem is solved using the Differential Evolution algorithm. A small case study is provided analysing the multi-class flow model and the strategy's application.

1. Introduction and background

A coordinated ramp metering optimal control strategy addressing global and local environmental policies in conjunction with operational efficiency and equity is designed here based on a newly developed multi-class macroscopic traffic flow model. The METANET model (*Modèle d' Écoulement sur le Traffic Autoroutier: NETworks*), (Kotsialos et al., 2002a), is extended to a multi-class version and is coupled with the pollutant emissions model COPERT, (Ntziachristos and Kouridis, 2007). Multi-class models are becoming an important extension of single-class models, since they yield a more detailed but still macroscopic description of traffic. They provide more details on the mechanism of congestion formation, shock wave propagation, capacity drop, flow synchronization, hysteresis, platoon dispersion, fundamental diagram scatter and other phenomena of interest to scientists and engineers, (Helbing and Treiber, 2002; Wong and Wong, 2002; Treiber and Helbing, 1999; Bellomo and Dogbe, 2011; Ngoduy, 2011; Coifman, 2015; Méndez et al., 2019).

Vehicle class oriented models are particularly suitable for considering the environmental impact of traffic when coupled with emissions models. The main emissions models used in conjunction with macroscopic flow models are COPERT, VERSIT + and VT-micro/macro. VT-macro (Zegeye et al., 2013) is based on the microscopic fuel consumption model VT-micro (Ahn, 1998) integrated with METANET. COPERT (Ntziachristos and Kouridis, 2007) is a family of average speed emissions models for a range of pollutants, fitted to data obtained from the field for vehicles of different engine standards and types of fuel. VERSIT + is based on a microscopic model (Smit et al., 2007; Ligterink et al., 2009), and relies on vehicle acceleration profiles (Pasquale et al., 2015a).

E-mail address: a.kotsialos@dei.com.gr.

Single-class macroscopic models consider the traffic stream as a homogeneous continuous medium aggregating all different vehicle classes in it. Multi-class models decompose this uniform stream into class-based macroscopic substreams using partial flows, densities and queues (and in case of a second-order model even partial mean speeds). For each substream, the dynamic equations of the single-class model are used, supplemented with a set of equations accounting for class-to-class interactions. The interaction mechanism depends on the specific modelling assumptions and the order of the original single-class model. Variants of first-order multi-class models can be found in (Wong and Wong, 2002; Loggne and Immers, 2008; van Lint et al., 2009; Tuerprasert and Aswakul, 2010; Ngoduy, 2010; Ngoduy, 2011; van Wageningen-Kessels et al., 2014; Qian et al., 2017). Multi-class extensions of the second-order model METANET (Kotsialos et al., 2002a) can be found in (Caligaris et al., 2007; Caligaris et al., 2010; Liu et al., 2014a; Pasquale et al., 2016b; Liu et al., 2014b; Chen et al., 2019; Liu et al., 2017; Deo et al., 2009), and of the Aw-Rascle-Zhang model (Aw and Rascle, 2000; Zhang, 2002) in (Bagnnerini and Rascle, 2003; Schnetzler and Louis, 2013; Balzotti et al., 2019). A detailed overview can be found in (van Wageningen-Kessels, 2013).

The notion of partial flows, densities and queues has been used in the past for single-class destination oriented models, e.g. (Papageorgiou, 1990; Kotsialos et al., 2002a). Destination oriented partial flows are useful for studying traffic assignment and designing route guidance controllers (Kotsialos et al., 2002b). Vehicle oriented partial flows are particularly useful for estimating pollutant emissions, which traffic management systems can utilise for implementing environmental policies.

Traffic management systems employ Ramp Metering (RM), Route Guidance (RG) and Variable Speed Limits (VSL) for pursuing efficiency, utilisation and environmental objectives (Papageorgiou et al., 2003; Kotsialos and Papageorgiou, 2004b). First-order multi-class models were used for designing RM strategies in (Schreiter et al., 2012; Schreiter et al., 2011; Liu et al., 2017), to name a few references, but since the model developed here is based on METANET we narrow our discussion to control designs based on it. RM in coordinated operation mode (CRM) is of interest here and the design method used is optimal control. Solutions of optimal control problems are used in the framework of Model Predictive Control (MPC), which is one of the most efficient approaches for managing road networks (Papageorgiou and Kotsialos, 2002).

Designing environmentally sustainable, equitable and operationally efficient MPC controllers requires understanding the relevance of the model used (Kotsialos and Papageorgiou, 2001). Single-class models have been used successfully for designing such strategies, e.g. for CRM efficiency and equity in (Kotsialos and Papageorgiou, 2004a) and for eco-friendly route guidance in (Luo et al., 2016), but a more detailed description of the environmental impact of traffic based on fuel consumption and emissions models is needed. From its early development, a model of fuel consumption was used by METANET for evaluating the environmental impact of implementing control measures, (Dynamic Systems and Simulation Laboratory, 2008); a more recent pollutant emissions model can be found in (Zegeye et al., 2013). An interesting combination of a fuel emission dispersion model with METANET is described in (Csikós et al., 2015; Csikós et al., 2018) in a single-class setting.

Multi-class models are highly relevant for addressing environmental objectives due to their ability to provide detailed maps of pollutant emissions from the various contributors. In Deo et al. (2009) the extension of METANET into a two-class version based on the notion of passenger car equivalence (*pce*) was proposed for developing integrated RM and VSL control. *pce* is a way of transforming class specific vehicle flow to equivalent flow of a reference class, typically the passenger car, (Transportation Research Board, 2000), and it was also used in the first-order model FASTLANE (van Wageningen-Kessels et al., 2014). A first-order model and METANET were used in (Liu et al., 2014a) for RM, which was extended in (Liu et al., 2016) where a robust scenario based rolling horizon MPC scheme for RM and VSL is described. In Liu et al. (2017) VT-macro and VERSIT + were combined with FASTLANE and METANET.

In Pasquale et al. (2014), a two-class extension of METANET was used for evaluating the local feedback RM strategy ALINEA (Papageorgiou et al., 1991) and its Proportional-Integral extension (Wang et al., 2010; Wang et al., 2014), using COPERT. In (Pasquale et al., 2015a) the results of applying the ALINEA type controllers using the VERSIT + emissions model, rather than COPERT, were reported. The two-class METANET model was used in (Pasquale et al., 2015b) for formulating an optimal control problem similar to the Advanced Motorway Optimal Control tool (Kotsialos and Papageorgiou, 2004c; Kotsialos et al., 2002b), with the cost criterion being the weighted sum of the total emissions and the Total Time Spent (TTS). The resulting problem was solved numerically using the Resilient Back Propagation algorithm (Riedmiller and Braun, 1993; Kotsialos, 2014). A similar approach was used in (Pasquale et al., 2016b) for designing an MPC controller, which includes a safety performance index in the cost criterion, without considering emissions.

In Pasquale et al. (2017a) the two-class extension of METANET was used with the VERSIT + model for calculating CO_2 emissions while controlling the network with RM and RG. The RM control approach was based on ALINEA applied on class-dedicated lanes and the approach followed for RG was to estimate the current anticipated travel time between two alternative routes for providing guidance aiming at dynamic user optimum conditions and VERSIT + for estimating emissions. This approach is similar to that described in (Pavlis and Papageorgiou, 1999) in its decentralised character. A heuristic supervision layer for achieving a cooperative effect on controller behaviour, an approach similar to the HERO (Papamichail et al., 2010b) RM strategy, was suggested in (Ferrara et al., 2017; Pasquale et al., 2018; Pasquale et al., 2020). Finally, a different approach based on multi-objective optimisation combining RM and VSL was suggested in (Chen et al., 2019), where the resulting optimisation problems are solved by stochastic search evolutionary algorithms. Clearly, multi-class combined with emissions model form an important part of ecological traffic management (Othman et al., 2019). A more detailed and recent review concerning traffic control with sustainability related objectives can be found in (Pasquale et al., 2019).

This paper contributes to the extant research by presenting a new multi-class modelling approach and an optimal control problem formulation for RM with both global and local environmental objectives, along with the usual efficiency and equity goals. Section 2 provides an overview of this paper's methodological approach. In Section 3, the multi-class extention of METANET is described in detail. The emissions models are briefly described in Section 4 along with two types of local environmental constraints incorporated in

the problem formulation, described in Section 5. The optimisation algorithm and the metrics used for evaluating a solution are given in Section 6. Section 7 presents the application of the overall system to a small test network. The results obtained are presented and discussed in Section 8. Section 9 summarises the conclusions of this paper and provides directions for future work.

2. General methodology and contributions

In prior work cited in Section 1, the approach followed for extending the single-class models to multi-class was to consider class-specific fundamental diagrams that become comparable due to *pce* scaling. The mixed traffic stream is divided into virtual substreams for each vehicle class with its dynamics modelled using the single-class model. Separate density, i.e. vehicle conservation equations, and fundamental diagram equations are used for each class and additionally for second-order models, separate empirical speed equations with class-specific relaxation, anticipation, merging and lane drop terms. This is illustrated in Fig. 1(a), where a traffic stream consisting of vehicles from five classes is split into five virtual substreams. For first-order models, the single mixed traffic dynamic density equation is replaced by partial density class-specific ones. For second-order, not only the density, but also, the speed equation is replaced by separate speed equations per class. The original single-class model is applied to the virtual substreams with the mixed fundamental diagram being the binding element modelling the influence of each class to the others.

Since traffic composition changes and evolves over time, the mixed fundamental diagram is a function of the partial densities and varies over time along with them. This is an important concept that departs from classic macroscopic models that assume a time, but not spatial, invariant equilibrium relationship (in the absence of VSL). For multi-class models this time invariance assumption does not apply any more and parameters change in every model time step.

An issue raised from the use of *pce*, relates to the fact that different vehicle classes may be equivalent in terms of traffic dynamics but very different in terms of environmental impact. For example, the mean driving and kinematic behaviour of a Euro1 petrol passenger car would be similar to a Euro5 diesel car, but their emissions would be very different. Following the approach of Fig. 1(a) requires the introduction of a different set of class equations for vehicles with the same average kinematics. This problem is overcome here by grouping together classes of vehicles that are the same from the perspective of macroscopic traffic dynamics but retain their differentiation with respect to emissions. The approach taken is illustrated in Fig. 1(b), where the mixed traffic stream is modelled macroscopically as a mixed stream consisting of the five individual classes and aggregating them into two general classes, passenger cars (*pc*) and trucks.

The emissions, though, are estimated based on the individual classes and a relevant global performance index is calculated. This calculation supports blanket environmental policies covering the entire network. However, Special Interest Areas (SIA) may exist in the network where authorities may require more flexible environmental policies with stricter regulations for specific time periods, e.g. near schools or hospitals for certain periods, rather than over the whole network and over the entire time horizon. In other words, as mentioned in (Lin et al., 2012), there may be a requirement for environmental policies to be applied at both the global and the local level. The introduction of such more specialised constraints is expected to reduce a CRM strategy's efficiency (Lin et al., 2016). Here, both types of policies are incorporated into the optimal control problem, which is solved by an evolutionary algorithm as suggested in an early version of the models discussed here, (Kotsialos, 2020).

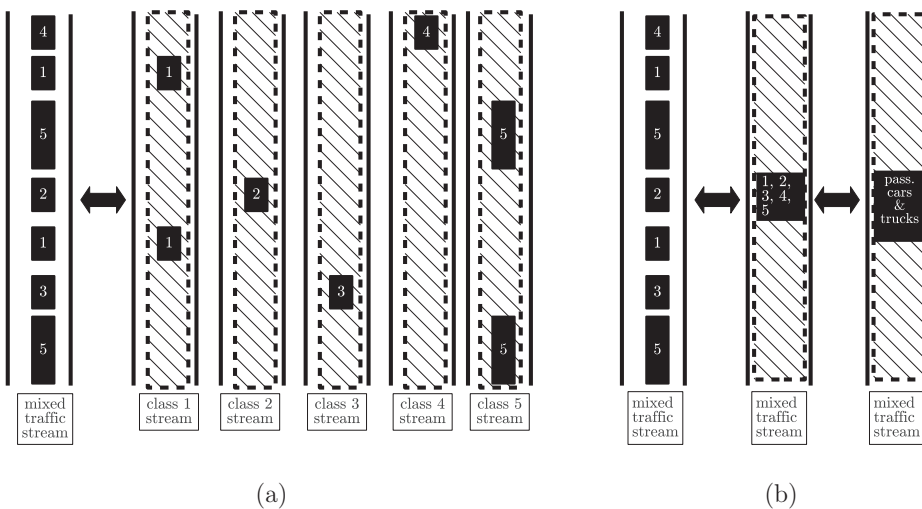


Fig. 1. Macroscopic multi-class modelling approaches for a traffic stream consisting of four passenger car classes and a truck class (hatching indicates macroscopic view of traffic). (a) Split into separate pure class substreams. (b) Mixed traffic stream of all classes viewed macroscopically as a single-class stream with varying model parameters; the different types of passenger cars and trucks are grouped into corresponding general classes for determining model parameters.

3. Traffic flow model development

3.1. Single-class motorway network model

A network of motorways is modelled as a directed graph $(\mathcal{N}, \mathcal{L})$ of nodes $n \in \mathcal{N}$ and links $\mu \in \mathcal{L}$. \mathcal{L} is divided into three subsets: \mathcal{L}_M of motorway, \mathcal{L}_O of origin and \mathcal{L}_D of destination links. Time is discretised into steps of length T_m indexed by k_m . A motorway link with l_μ lanes is divided into S_μ segments of equal length Δ_μ . Traffic conditions in segment (μ, i) are described by the vehicle density $\rho_{\mu,i}$ (veh/km/lane), space mean speed $v_{\mu,i}$ (km/h) and vehicle flow $q_{\mu,i}$ (veh/h). The dynamics of traffic are described by the following equations:

$$\rho_{\mu,i}(k_m + 1) = \rho_{\mu,i}(k_m) + \frac{T_m}{\Delta_\mu l_\mu} [q_{\mu,i-1}(k_m) - q_{\mu,i}(k_m)] \quad (1)$$

$$v_{\mu,i}(k_m + 1) = v_{\mu,i}(k_m) + T_m \text{sat} \left\{ \sum_{\chi \in \mathcal{X}} \text{sat} \left[g_{\mu,i}^{(\chi)}(k_m) \right] \right\} \quad (2)$$

$$V[\rho_{\mu,i}(k_m)] = v_{\mu,i,\max} \exp \left\{ - \frac{1}{a_{\mu,i}} \left[\frac{\rho_{\mu,i}(k_m)}{\rho_{\mu,i,cr}} \right]^{a_{\mu,i}} \right\} \quad (3)$$

$$q_{\mu,i}(k_m) = \rho_{\mu,i}(k_m) v_{\mu,i}(k_m) l_\mu \quad (4)$$

where $\rho_{\mu,i,cr}$ (veh/km/lane) the critical density, $v_{\mu,i,\max}$ (km/h) the free flow speed and $a_{\mu,i}$ (no units) are segment specific parameters of the fundamental diagram V (km/h) and $\chi \in \mathcal{X} = \{(relax), (conv), (antic), (merge), (drop)\}$ is an index of the acceleration processes that contribute towards the total speed update in (2). These are

$$\text{relaxation} : g_{\mu,i}^{(relax)}(k_m) = \frac{1}{\tau_{\mu,i}} \{ V[\rho_{\mu,i}(k_m)] - v_{\mu,i}(k_m) \} \quad (5)$$

$$\text{convection} : g_{\mu,i}^{(conv)}(k_m) = \frac{1}{\Delta_\mu} v_{\mu,i}(k_m) [v_{\mu,i-1}(k_m) - v_{\mu,i}(k_m)] \quad (6)$$

$$\text{anticipation} : g_{\mu,i}^{(antic)}(k_m) = \frac{\nu_{\mu,i}}{\Delta_\mu \tau_{\mu,i}} \frac{\rho_{\mu,i}(k_m) - \rho_{\mu,i+1}(k_m)}{\rho_{\mu,i}(k_m)} \quad (7)$$

$$\text{on-ramp merge} : g_{\mu,i}^{(merge)}(k_m) = -\delta_{\mu,i} \frac{q_{o,out}(k_m) v_{\mu,1}(k_m)}{\Delta_\mu l_\mu \rho_{\mu,1}(k_m)} \quad (8)$$

$$\text{lane drop} : g_{\mu,i}^{(drop)}(k_m) = -\phi_{\mu,i} \frac{(l_{\mu_2} - l_{\mu_1}) \rho_{\mu_1,S_{\mu_1}(k_m)} v_{\mu_1,S_{\mu_1}}(k_m)^2}{\Delta_\mu l_{\mu_1} \rho_{\mu_1,cr}} \quad (9)$$

where $\tau_{\mu,i}$ (h), $v_{\mu,i}$ (km²/h), $\delta_{\mu,i}$ (no units), $\phi_{\mu,i}$ (no units) are relaxation, anticipation, merging and drop of lanes parameters, $q_{o,out}(k_m)$ in (8) in the merge term is the flow from origin o to the first segment of the downstream road link μ , and μ_1 and μ_2 in (9) are the upstream and downstream connected links where a lane drop occurs. The saturation operator used in (2) bounds the acceleration of each separate process within an upper and a lower limit, $g_{\min} > 0$ (km/h²) and $g_{\max} > 0$ (km/h²), i.e.

$$\text{sat}(g) = \begin{cases} g_{\max} & \text{if } g > g_{\max} \\ g & \text{if } -g_{\min} \leq g \leq g_{\max} \\ -g_{\min} & \text{if } g < -g_{\min}. \end{cases} \quad (10)$$

Traffic conditions in an origin link $o \in \mathcal{L}_O$ are described by a linear model of the queue length w_o (veh). Queues depend on the exogenous demand d_o (veh/h) generated in the environment, the downstream link μ traffic conditions and whether or not ramp metering control measures are applied. The queue dynamics are

$$w_o(k_m + 1) = w_o(k_m) + T_m [d_o(k_m) - q_{o,out}(k_m)] \quad (11)$$

where $q_{o,out}(k_m)$ is the realised ramp outflow given from

$$q_{o,out}(k_m) = \min \{ q_o^{(1)}(k_m), q_o^{(2)}(k_m) \} \quad (12)$$

with

$$q_o^{(1)} = \min \left\{ d_o + \frac{w_o}{T_m}, Q_{o,\max} \right\} \text{ and } q_o^{(2)} = Q_{o,\max} \min \left\{ 1, \frac{\rho_{\mu,1,\max} - \rho_{\mu,1}}{\rho_{\mu,1,\max} - \rho_{\mu,1,cr}} \right\} \quad (13)$$

where $Q_{o,\max}$ (veh/h) the maximum possible outflow from o and $\rho_{\mu,1,\max}$ (veh/km/lane) the maximum density of the downstream segment.

For a destination link $b \in \mathcal{L}_D$, the outflow $q_{b,\text{exit}}(k_m)$ (veh/h) is the flow sent to the environment, assumed to have infinite capacity. If $n \in \mathcal{N}$ is the node where b is attached

$$q_{b,\text{exit}}(k_m) = q_{n,b,0}(k_m) \quad (14)$$

where $q_{n,b,0}(k_m)$ (veh/h) is calculated by the node model (see eqns. (20) and (32)).

The static node model provides a mechanism for calculating $v_{\mu,1}$ needed in (6) for $i = 1$ and $\rho_{\mu,i+1}$ in (7) for $i = S_\mu$. It also distributes the total incoming flow at a node to the outgoing links. Only three possible node topologies are considered, the 1-in-1-out, the 2-in-1-out and the 1-in-2-out links, Fig. 2.

Node n assumes a mean speed $v_n(k_m)$ and density $\rho_n(k_m)$, used in (6) and (7), respectively. The incoming flow $q_{n,\text{in}}(k_m)$ (veh/h) is the total flow coming in the node during period k_m and the node outflow to the exit link μ is $q_{n,\mu,0}(k_m)$ (veh/h), which is used in (1). Depending on the node's topology and referring to the symbols of Fig. 2 these quantities are calculated as follows for each possible configuration:

- 1-in-1-out (Fig. 2(a)):

– $\mu_1, \mu_2 \in \mathcal{L}_M$. In this case

$$v_n(k_m) = v_{\mu_1,S_{\mu_1}}(k_m) \quad (15)$$

$$\rho_n(k_m) = \rho_{\mu_1}(k_m) \quad (16)$$

$$q_{n,\text{in}}(k_m) = q_{\mu_1,S_{\mu_1}}(k_m) \quad (17)$$

$$q_{n,\mu_2,0}(k_m) = q_{n,\text{in}}(k_m) \quad (18)$$

– $\mu_1 \in \mathcal{L}_O$ and $\mu_2 \in \mathcal{L}_M$. In this case, v_n is not defined and the convection term (6) in (2) is omitted. The downstream density used by the origin link model in (13) is given from (16). The node flows are

$$q_{n,\text{in}}(k_m) = q_{\mu_1,\text{out}}(k_m) \quad (19)$$

and $q_{n,\mu_2,0}(k_m)$ is given from (18).

– $\mu_1 \in \mathcal{L}_M$ and $\mu_2 \in \mathcal{L}_D$. In this case, there is no need to define a node speed. The node density is set to zero, i.e. $\rho_n(k_m) = 0$. $q_{n,\text{in}}(k_m)$ is given from (17) and $q_{n,\mu_2,0}(k_m)$ from (18). Therefore

$$q_{\mu_2,\text{exit}}(k_m) = q_{n,\mu_2,0}(k_m). \quad (20)$$

- 2-in-1-out (Fig. 2(b)):

– $\mu_1, \mu_2, \mu_3 \in \mathcal{L}_M$. In this case

$$v_n(k_m) = \frac{\sum_{\mu=\mu_1, \mu_2} q_{\mu,S_\mu}(k_m) v_{\mu,S_\mu}(k_m)}{\sum_{\mu=\mu_1, \mu_2} v_{\mu,S_\mu}(k_m)} \quad (21)$$

$$\rho_n(k_m) = \rho_{\mu_3,1}(k_m) \quad (22)$$

$$q_{n,\text{in}}(k_m) = \sum_{\mu=\mu_1, \mu_2} q_{\mu,S_\mu}(k_m) \quad (23)$$

$$q_{n,\mu_3,0}(k_m) = q_{n,\text{in}}(k_m). \quad (24)$$

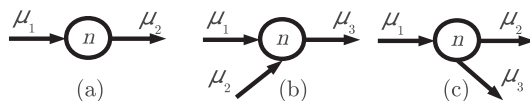


Fig. 2. Traffic flow model node topologies.

$\mu_1, \mu_3 \in \mathcal{L}_M, \mu_2 \in \mathcal{L}_O$. In this case

$$v_n(k_m) = v_{\mu_1, S_{\mu_1}}(k_m) \quad (25)$$

$$q_{n,in}(k_m) = q_{\mu_1, S_{\mu_1}}(k_m) + q_{\mu_2, out}(k_m) \quad (26)$$

and (22) and (24) give the node density and μ_3 's upstream flow, respectively.

- 1-in-2-out (Fig. 2(c)): For this node topology the turning rates $\beta_{n,\mu_2}(k_m)$ and $\beta_{n,\mu_3}(k_m)$ are used, with

$$\beta_{n,\mu}(k_m) = \frac{q_{n,\mu,0}(k_m)}{q_{n,in}(k_m)}, \mu = \mu_2, \mu_3 \text{ and therefore} \quad (27)$$

$$\beta_{n,\mu_2}(k_m) + \beta_{n,\mu_3}(k_m) = 1. \quad (28)$$

The turning rates are disturbance trajectories provided as input.

$\mu_1, \mu_2, \mu_3 \in \mathcal{L}_M$. Then

$$v_n(k_m) = v_{\mu_1, S_{\mu_1}}(k_m) \quad (29)$$

$$\rho_n(k_m) = \frac{\sum_{\mu=\mu_2, \mu_3} \rho_{\mu,1}(k_m)^2}{\sum_{\mu=\mu_2, \mu_3} \rho_{\mu,1}(k_m)} \quad (30)$$

$$q_{n,in}(k_m) = q_{\mu_1, S_{\mu_1}}(k_m) \quad (31)$$

$$q_{n,\mu,0}(k_m) = \beta_{n,\mu}(k_m) q_{n,in}(k_m), \mu = \mu_2, \mu_3. \quad (32)$$

$\mu_1, \mu_2 \in \mathcal{L}_M, \mu_3 \in \mathcal{L}_D$. In this case the node speed is given from (29) and

$$\rho_n(k_m) = \rho_{\mu_2,1}(k_m) \quad (33)$$

and the flows from (31), (32) and (14).

$\mu_1 \in \mathcal{L}_O, \mu_2, \mu_3 \in \mathcal{L}_M$. In this case, the node speed is not defined and the convection term (6) is not included in (2) for segments $(\mu_2, 1)$ and $(\mu_3, 1)$. The node inflow is given from (19) and the outflows from (32).

The application of (32) implies the same turning behaviour of pc and trucks and the turning rate is applied to all vehicle classes, hence the “cross-class” characterisation.

The 2-in-1-out case with $\mu_1 \in \mathcal{L}_O$ and $\mu_2 \in \mathcal{L}_O$ is not considered here, although it models a meaningful situation when the purpose is to model two different queues connected with the motorway at the same location. The rest of the possible configurations are either not meaningful or can be considered by the ones visited.

3.2. From single-class to multi-class

Let \mathcal{J} denote the set of vehicle classes and j its index. Each class j has its own characteristics including, length, fuel type, maximum speed, acceleration/deceleration capabilities and typical load. The acceleration/deceleration capability of each vehicle class dictates the values of g_{min} and g_{max} used in (10). Let $g_{j,min} > 0$ (km/h^2) and $g_{j,max} > 0$ (km/h^2) the maximum deceleration (in absolute value) and maximum acceleration of class j , respectively. Then,

$$g_{min} = \max_{j \in \mathcal{J}} \{g_{j,min}\} \text{ and } g_{max} = \max_{j \in \mathcal{J}} \{g_{j,max}\}. \quad (34)$$

Given g_{min} and g_{max} , the model time step is selected so that the following condition is satisfied:

$$T_m \leq \min \left\{ \min_{\mu \in \mathcal{S}_M} \left\{ \frac{\Delta_\mu}{\min_{j \in \mathcal{J}} v_{j,\max}} \right\}, \min_{j \in \mathcal{J}} \left\{ \frac{v_{j,\max}}{g_{j,\max}} \right\}, \min_{j \in \mathcal{J}} \left\{ \frac{v_{j,\max}}{g_{j,\min}} \right\} \right\}. \quad (35)$$

The first term in the minimum operator of the left side of (35) is based on the Courant-Friedrichs-Levy condition that is always observed in the single-class models, whereas the other two terms are introduced to prevent unrealistic acceleration profiles in a motorway segment for a particular vehicle class. $v_{j,\max}/g_{j,\max}$ is the time it takes a vehicle of class j to reach its maximum speed using maximum acceleration from rest, and $v_{j,\max}/g_{j,\min}$ is the time it takes to reach rest from maximum speed using maximum deceleration. Selecting a T_m that respects (35) is a conservative choice that allows vehicles to complete these manoeuvres in a single time step.

The single-class model has a number of parameters related to the fundamental diagram (3), the speed Eq. (2) and the on-ramp capacity (13). These are $\rho_{\mu,i,cr}, a_{\mu,i}, \tau_{\mu,i}, \nu_{\mu,i}, \phi_{\mu,i}, \delta_{\mu,i}, Q_{o,\max}$, which are identified by a rigorous model validation procedure (Kotsialos et al., 2002a; Poole and Kotsialos, 2016b,a; Poole and Kotsialos, 2018). The motorway link geometric homogeneity allows the use of the same set of model parameter values for all segments of a link. However, the introduction of the vehicle class as a separate model element results to varying flow composition and consequently to changes of the model parameters' values at the segment level. In order to model this effect, the notion of the vehicle class composition rate is introduced.

The vehicle class composition rate of a motorway segment $(\mu, i), \gamma_{\mu,i,j}(k_m) \in [0, 1]$ is the number of vehicles of class $j \in \mathcal{J}$ in (μ, i) at time $k_m T_m$ over the total number of vehicles in that segment. For an origin link $o \in \mathcal{L}_O, \gamma_{o,j}(k_m) \in [0, 1]$ is the number of vehicles of class j over the total number of vehicles waiting in the queue. For $o \in \mathcal{L}_O, \theta_{o,j}(k_m) \in [0, 1]$ is the part of the demand originating from the environment at o during period k_m that consists of vehicles belonging to class j .

Let \mathbf{p}_m be a suitably dimensioned vector where all model parameters are collected, with

$$\mathbf{p}_m = [\rho_{cr}^\top \mathbf{v}_{\max}^\top \mathbf{a}^\top \boldsymbol{\tau}^\top \boldsymbol{\nu}^\top \boldsymbol{\delta}^\top \boldsymbol{\phi}^\top \mathbf{Q}_{\max}^\top]^\top \quad (36)$$

where $\rho_{cr} = [\dots \rho_{\mu,1,cr} \dots \rho_{\mu,S_\mu,cr} \dots]^\top, \mathbf{v}_{\max} = [\dots v_{\mu,1,\max} \dots v_{\mu,S_\mu,\max} \dots]^\top, \mathbf{a} = [\dots a_{\mu,1} \dots a_{\mu,S_\mu} \dots]^\top, \boldsymbol{\tau} = [\dots \tau_{\mu,1} \dots \tau_{\mu,S_\mu} \dots]^\top, \boldsymbol{\nu} = [\dots \nu_{\mu,1} \dots \nu_{\mu,S_\mu} \dots]^\top, \boldsymbol{\delta} = [\delta_{\mu_1,1} \dots \delta_{\mu_{F_1},1}]^\top$, μ_1, \dots, μ_{F_1} links with an on-ramp upstream, $\boldsymbol{\phi} = [\phi_{\mu_1,S_{\mu_1}} \dots \phi_{\mu_{F_2},S_{\mu_{F_2}}} \dots]^\top$, μ_1, \dots, μ_{F_2} links with downstream lanedrop, $\mathbf{Q}_{\max} = [Q_{1,\max} \dots Q_{|\mathcal{L}_O|,\max}]^\top$.

In the modelling approach followed here, the assumption of time-invariance of the model parameters is dropped and a mechanism is established for determining how \mathbf{p}_m changes along with the evolving composition of traffic. Thus, \mathbf{p}_m becomes $\mathbf{p}_m(\gamma(k_m))$, where γ is a suitably dimensioned vector of the network's compositions rates. Similar to (van Wageningen-Kessels et al., 2014; Pasquale et al., 2017b; Pasquale et al., 2015a,b), two general vehicle classes are further considered, *pc* and trucks. From the macroscopic traffic dynamics perspective *pc* subclasses are identical. Let $\mathcal{J}_{pc} \subseteq \mathcal{J}$ be the index set of the *pc* subclasses and \mathcal{J}_{tr} the index set of trucks subclasses. The *pc* class composition rate $\Gamma_{\mu,i,1}$ for segment (μ, i) is

$$\Gamma_{\mu,i,1}(k_m) = \sum_{j \in \mathcal{J}_{pc}} \gamma_{\mu,i,j}(k_m) \quad (37)$$

and the corresponding composition rate for trucks with index $j \in \mathcal{J}_{tr}$ is

$$\Gamma_{\mu,i,2}(k_m) = \sum_{j \in \mathcal{J}_{tr}} \gamma_{\mu,i,j}(k_m). \quad (38)$$

A similar definition applies for origin queues and demand trajectories. Clearly,

$$\Gamma_{\varsigma,1}(k_m) + \Gamma_{\varsigma,2}(k_m) = 1 \quad (39)$$

where ς a location index, i.e. segment (μ, i) or origin o . Let $\boldsymbol{\Gamma}_1$ be the vector where the *pc* composition rates are collected and $\boldsymbol{\Gamma}_2$ the analogous vector of the trucks'. It is straightforward to change \mathbf{p}_m 's dependence from γ to $\boldsymbol{\Gamma}$, i.e. to $\mathbf{p}_m[\boldsymbol{\Gamma}_1(k_m), \boldsymbol{\Gamma}_2(k_m)]$, which is monotonic with respect to $\boldsymbol{\Gamma}_1(k_m)$ and $\boldsymbol{\Gamma}_2(k_m)$ and therefore in view of (39), $\mathbf{p}_m[\boldsymbol{\Gamma}_1(k_m), \boldsymbol{\Gamma}_2(k_m)] = \mathbf{p}_m[\boldsymbol{\Gamma}_1(k_m)]$.

A particular model parameter is bounded and varies continuously and monotonically within $[p_{m,\varsigma}^{(1)}, p_{m,\varsigma}^{(2)}]$; these two bounds are the parameter's value when the traffic flow consists of only one general class of vehicles and can take either the value $p_{m,\varsigma}(0, 1)$ or $p_{m,\varsigma}(1, 0)$ as shown in Table 1. The critical density at (μ, i) assumes its largest value when only *pc* exist in the traffic stream, i.e. when $(\Gamma_{\mu,i,1}, \Gamma_{\mu,i,2}) = (1, 0)$, whereas it attains its lowest when there are only trucks in it, i.e. when $(\Gamma_{\mu,i,1}, \Gamma_{\mu,i,2}) = (0, 1)$. The same is true for the maximum

Table 1
Parameter lower and upper bounds as functions of composition rates.

$p_{m,\varsigma}^{(1)}$	$p_{m,\varsigma}^{(2)}$	$p_{m,\varsigma}^{(1)}$	$p_{m,\varsigma}^{(2)}$
$\rho_{\varsigma,cr}(0, 1)$	$\rho_{\varsigma,cr}(1, 0)$	$a_{\varsigma}(1, 0)$	$a_{\varsigma}(0, 1)$
$v_{\varsigma,\max}(0, 1)$	$v_{\varsigma,\max}(1, 0)$	$\tau_{\varsigma}(1, 0)$	$\tau_{\varsigma}(0, 1)$
$\nu_{\varsigma}(1, 0)$	$\nu_{\varsigma}(0, 1)$	$\delta_{\varsigma}(1, 0)$	$\delta_{\varsigma}(0, 1)$
$\phi_{\varsigma}(1, 0)$	$\phi_{\varsigma}(0, 1)$	$Q_{\varsigma,\max}(0, 1)$	$Q_{\varsigma,\max}(1, 0)$

speed of the fundamental diagram. The reverse happens for the $a_{\mu,i}$ exponent, i.e. pure truck traffic has a larger $a_{\mu,i}$ than pure pc. The results of this argument can be seen in Fig. 3, where the flow-density and speed-density fundamental diagrams are shown for pure pc and pure truck traffic. The shape of the displayed curves is consistent with theoretical and empirical models, e.g. (Méndez et al., 2019; Helbing and Treiber, 2002). Regarding the relaxation time, it is smaller for pc and larger for trucks, with the argument been that pc are more agile and can adjust faster in the prevailing traffic conditions. Also, truck traffic is considered more anticipative than pc's, (van Wageningen-Kessels et al., 2014). Furthermore, the impact on the mean speed of on-ramp merging is larger for the truck traffic than for pc and the same is assumed for the lane drops.

In reality due to complex car-following microscopic interactions, it takes only a few trucks scattered in a segment's area to significantly affect and change its local traffic flow characteristics. The heavier the traffic is, the faster and more prominent the trucks' influence, even when in small numbers. This suggests a strongly nonlinear relationship between the parameters used for modelling the flow characteristics, the traffic composition and the total number of vehicles contained within the segment. The approach followed here, is to use the logistic (or sigmoid) curve for representing this nonlinear relationship. The logistic growth (and decay) model provides a flexible and powerful component, in the overall multi-class model, that has the potential to capture accurately the strong nonlinearities of the traffic characteristics' dynamics.

Let $\sigma[\Gamma_{\varsigma,1}(k_m)] \in [0, 1]$ be the sigmoid weight function with

$$\sigma[\Gamma_{\varsigma,1}(k_m)] = \left[\{1 + \exp\{-\psi_1[\Gamma_{\varsigma,1}(k_m) - \psi_2]\}\}^{1/\psi_3} \right]^{-1} \quad (40)$$

where ψ_1, ψ_2 and ψ_3 are quantities characterising $p_{m,\varsigma}$. For a given density (queue) level, $p_{m,\varsigma}[\Gamma_{\varsigma,1}(k_m)]$ is calculated as a function of the pc composition rate as

$$p_{m,\varsigma}[\Gamma_{\varsigma,1}(k_m)] = \sigma[\Gamma_{\varsigma,1}(k_m)] p_{m,\varsigma}[\Gamma_{\varsigma,1}(k_m)] + \{1 - \sigma[\Gamma_{\varsigma,1}(k_m)]\} p_{m,\varsigma}[1 - \Gamma_{\varsigma,1}(k_m)]. \quad (41)$$

The values of ψ_1, ψ_2 and ψ_3 reflect how each model parameter changes over traffic composition and are parameter-specific. Fig. 4 shows the dependence of the critical density (a) and the relaxation time (b) at a location ς on the passenger composition rate $\Gamma_{\varsigma,1}$. The critical density of a pure passenger car traffic stream is $\rho_{\varsigma,cr}(1, 0) = 33$ (veh/km/lane), whereas of a pure truck traffic stream is $\rho_{\varsigma,cr}(0, 1) = 24$ (veh/km/lane). Both subfigures show curves for different values of the triplet (ψ_1, ψ_2, ψ_3) , which governs the inflection point and the rate at which the parameter changes with the pc composition rates.

These curves show the parameters' dependence on the composition rate for a fixed level of density. However, the denser the overall traffic, the more dominant the effect of truck traffic. In order to model this effect, the parameter ψ_2 is set to be a function of the segment density $\rho_{\mu,i}(k_m)$ in the form

$$\psi_2[\rho_{\mu,i}(k_m)] = \psi_2^{(0)} + (1 - \psi_2^{(0)}) \frac{\rho_{\mu,i}(k_m)}{\rho_{\max}^{(0)} l_\mu} \quad (42)$$

where $\psi^{(0)}$ and $\rho_{\max}^{(0)}$ are suitable parameters. The rationale behind this relationship is based on the observation that as ψ_2 increases the truck traffic becomes more dominant with increasing $\Gamma_{\mu,i,1}$, i.e. a smaller truck composition has greater effect as ψ_2 in (40) increases. Notice that the impact of increasing density is depreciated by the segment's number of lanes, partially accounting for increased speed at lanes with fewer trucks. Fig. 5 depicts the surfaces for the critical density in (a) and the relaxation time in (b). The resulting fundamental diagram with parameters calculated according to (41) is shown in Fig. 5(c). Such 3-dimensional fundamental diagrams have been proposed in the literature, e.g. in (Persaud and Hall, 1989; Hall, 1996; Delle Monache et al., 2018), where they are spanned over flow, occupancy and speed or density, and in the framework of multi-class modelling in (Chanut and Buisson, 2003). Clearly, for

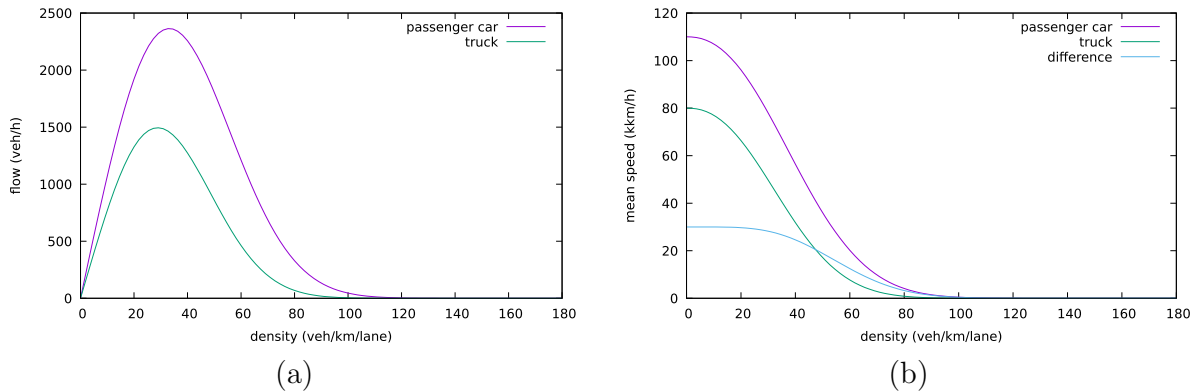


Fig. 3. (a) Flow–density and (b) speed–density relationships for pure pc and truck traffic.

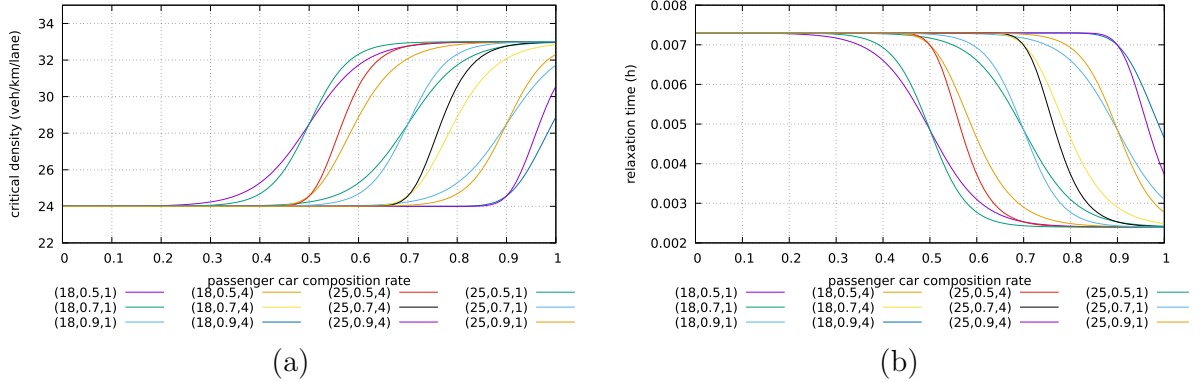


Fig. 4. Dependence on passenger car composition rates of: (a) critical density and (b) relaxation time.

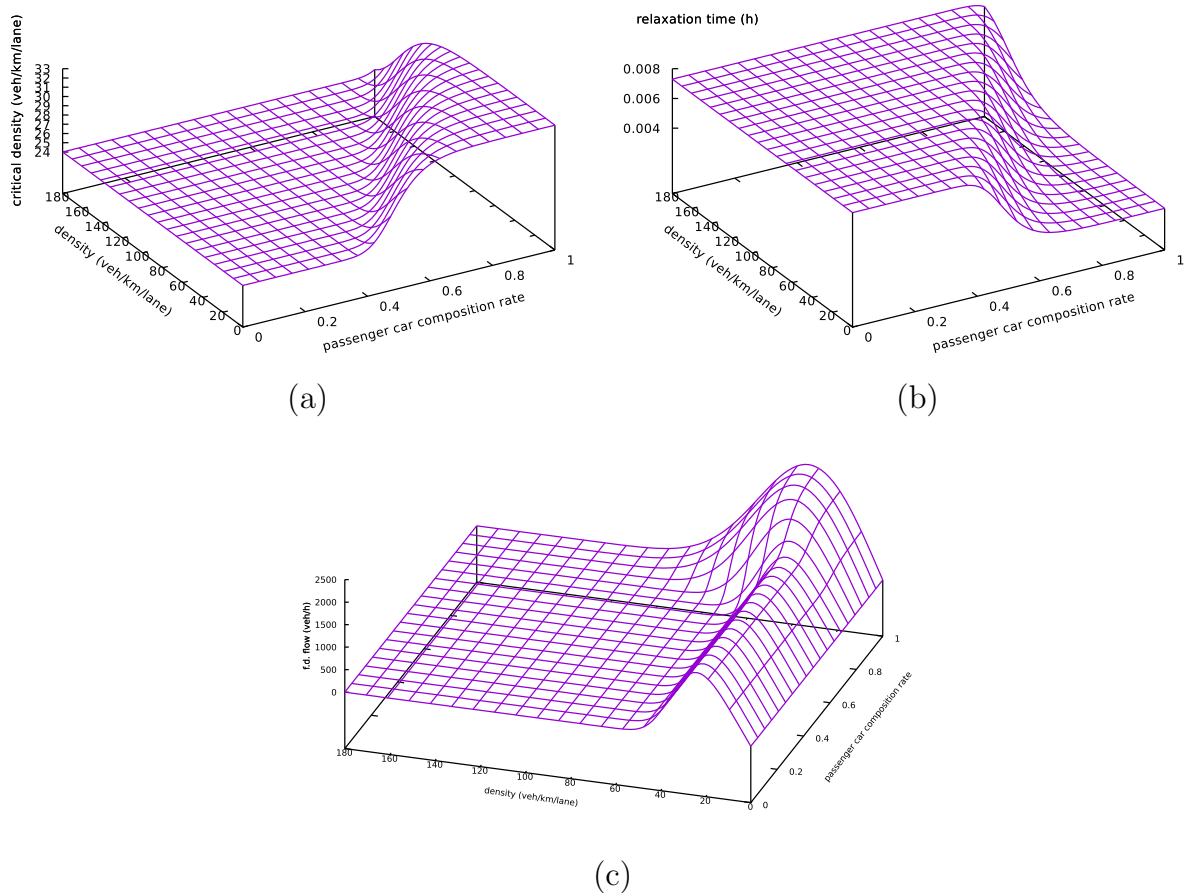


Fig. 5. (a) Critical density and (b) relaxation time dependence on passenger car composition and overall density. (c) Fundamental diagram for $(\psi_1, \psi_2^{(0)}, \psi_3) = (18, 0.7, 4)$ applied to parameters $\rho_{\mu,i,cr}, v_{\mu,i,max}$ and $a_{\mu,i}$.

any practical application $p_{m,\zeta}^{(1)}, p_{m,\zeta}^{(2)}$ and $(\psi_1, \psi_2^{(0)}, \psi_3)$, should be estimated for each parameter by a rigorous model validation in the line of (Poole and Kotsialos, 2016a; Poole and Kotsialos, 2018).

3.3. Vehicle oriented dynamic traffic flow model

The dynamic models of partial flow, densities and queues rest on the assumption of uniform cross-class flow discharge, i.e. that the outflow from any segment (origin link) has the same composition as that of the whole segment (queue). This is a rather strong assumption, which can be relaxed, but facilitates model development.

Let us define now the state variable partial density per vehicle class j in segment $(\mu, i), y_{\mu,i,j}(k_m)$ as

$$y_{\mu,i,j}(k_m) = \gamma_{\mu,i,j}(k_m) \rho_{\mu,i}(k_m). \quad (43)$$

Then vehicle conservation yields

$$y_{\mu,i,j}(k_m + 1) = y_{\mu,i,j}(k_m) + \frac{T_m}{\Delta_\mu l_\mu} [q_{\mu,i-1,j}(k_m) - q_{\mu,i,j}(k_m)] \quad (44)$$

with the partial outflows satisfying $\sum_{j \in J} q_{\mu,i,j}(k_m) = q_{\mu,i}(k_m)$. The cross-class uniform segment outflow assumption implies that all vehicles in the segment of both general classes have the same speed, i.e.

$$q_{\mu,i,j}(k_m) = \gamma_{\mu,i,j}(k_m) q_{\mu,i}(k_m) \stackrel{(4)}{=} \gamma_{\mu,i,j}(k_m) \rho_{\mu,i}(k_m) v_{\mu,i}(k_m) l_\mu \stackrel{(43)}{=} y_{\mu,i,j}(k_m) v_{\mu,i}(k_m) l_\mu \quad (45)$$

which results to the partial densities dynamic equation

$$y_{\mu,i,j}(k_m + 1) = y_{\mu,i,j}(k_m) + \frac{T_m}{\Delta_\mu} [y_{\mu,i-1,j}(k_m) v_{\mu,i-1}(k_m) - y_{\mu,i,j}(k_m) v_{\mu,i}(k_m)]. \quad (46)$$

When $i = 1$, Eq. (46) is suitably adapted to the node topology. If one of the upstream links is an origin o , then the term $y_{\mu,S_\mu,j}(k_m) v_{\mu,S_\mu}(k_m) l_\mu$ corresponding to $\mu = o$ is replaced by $\gamma_{o,j}(k_m) q_{o,out}(k_m)$.

The state variable partial queues per class j of origin o , $y_{o,j}(k_m)$ are defined as

$$y_{o,j}(k_m) = \gamma_{o,j}(k_m) w_o(k_m) \quad (47)$$

and based on vehicle conservation

$$y_{o,j}(k_m + 1) = y_{o,j}(k_m) + T_m [\theta_{o,j}(k_m) d_o(k_m) - q_{o,out,j}(k_m)] \quad (48)$$

with $\sum_{j \in J} q_{o,out,j}(k_m) = q_{o,out}(k_m)$. The assumption of cross-class uniform queue outflow results to

$$q_{o,out,j}(k_m) = \begin{cases} \frac{q_{o,out}(k_m)}{d_o(k_m) + \frac{w_o(k_m)}{T_m}} \left[\theta_{o,j}(k_m) d_o(k_m) + \frac{y_{o,j}(k_m)}{T_m} \right] & \text{if } d_o(k_m) + \frac{w_o(k_m)}{T_m} > 0 \\ 0 & \text{if } d_o(k_m) + \frac{w_o(k_m)}{T_m} = 0. \end{cases} \quad (49)$$

and therefore from (48)

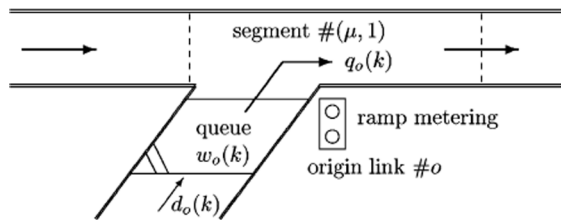


Fig. 6. The origin ramp metering setting.

$$y_{o,j}(k_m + 1) = \begin{cases} \left[1 - \frac{q_{o,out}(k_m)}{d_o(k_m) + \frac{w_o(k_m)}{T_m}} \right] [y_{o,j}(k_m) + T_m \vartheta_{o,j}(k_m) d_o(k_m)] & \text{if } d_o(k_m) + \frac{w_o(k_m)}{T_m} > 0 \\ 0 & \text{if } d_o(k_m) + \frac{w_o(k_m)}{T_m} = 0. \end{cases} \quad (50)$$

Eqs. (44) and (48) are valid even without the uniform outflow assumption. If this is the case, (46) and (50) can be replaced by a deterministic outflow calculation protocol or a stochastic sampling scheme, that depend on traffic composition and conditions. This is left for future development.

3.4. Ramp metering operation

Referring to Fig. 6, the RM problem is to calculate for every model time step k_m a rate $r_o(k_m) \in [r_{\min}, 1]$, where r_{\min} a preset minimum. When $r_o(k_m)$ is applied on $q_{o,out}(k_m)$ the regulated ramp outflow $q_o(k_m)$ is

$$q_o(k_m) = r_o(k_m) q_{o,out}(k_m). \quad (51)$$

Thus, for metered on-ramps the term $q_{o,out}(k_m)$ in Eqns. (11), (8), (19), (50) and (49) is replaced by $q_o(k_m)$.

Let T_c (h) be the time interval between two consecutive decisions about the value of the RM rate. Typically, T_c is larger than the model time step T_m and depends on the equipment used, regulations and RM policies (variable green phase duration with fixed cycle, (# of)-cars-per-green, discrete release rates (Kotsialos et al., 2006)). For simplifying the source code implementation, it is assumed that

$$\frac{T_c}{T_m} = \alpha_{cm} \in \mathbb{N}^*. \quad (52)$$

A RM rate is calculated every α_{cm} model time steps and in between it is assumed constant. Let k_c be the time step index counting control (as opposed to model) time steps. The RM strategy algorithm is invoked every step k_c and the resulting $r_o(k_c)$ is communicated back to the model without any delay and is applied constantly for the next α_{cm} model time steps. A known k_m belongs to control time step k_c given from

$$k_c = \lfloor \frac{k_m}{\alpha_{cm}} \rfloor \quad (53)$$

Thus, the rate plugged-in (51) is given from

$$r_o(k_m) = r_o \left(\left\lfloor \frac{k_m}{\alpha_{cm}} \right\rfloor \right) \quad (54)$$

after the RM strategy calculates $r_o(k_c)$.

4. Emissions and environmental policies

4.1. COPERT emissions models

The basis for calculating environmental related performance measures is the well known COPERT family of models (Ntziachristos and Kouridis, 2007). Other emissions models like those mentioned in Section 1 or even more updated ones can be used as well.

Let \mathcal{Z} be the index set of pollutants of interest, e.g. CO, NO_x , and let z be the corresponding index. For a particular pollutant $z \in \mathcal{Z}$ and class of vehicles $j \in \mathcal{J}$ the amount $\Xi_{j,z}(v)$ (grams/km/veh) of emissions are calculated as a function of the mean speed v . $\Xi_{j,z}(v)$ are given analytically for passenger cars as

$$\Xi_{j,z}(v) = \frac{\xi_{j,z}^{(1)} + \xi_{j,z}^{(2)} v + \xi_{j,z}^{(3)} v^2}{1 + \xi_{j,z}^{(4)} v + \xi_{j,z}^{(5)} v^2} \quad (55)$$

and for trucks (using the index j') as

$$\Xi_{j',z}(v) = \xi_{j',z}^{(1)} + \frac{\xi_{j',z}^{(2)}}{1 + \exp[-\xi_{j',z}^{(3)} + \xi_{j',z}^{(4)} \ln(v) + \xi_{j',z}^{(5)} v]} \quad (56)$$

where $\xi_{j,z}^{(1)}, \dots, \xi_{j,z}^{(5)}, j, j' \in \mathcal{J}$ and $z \in \mathcal{Z}$ are COPERT model parameters estimated from experimental field investigations.

The emissions of vehicles of class j in (μ, i) during step $k_m, E_{\mu,i,j,z}(k_m)$ (grams) are

$$E_{\mu,i,j,z}(k_m) = \Delta_\mu l_\mu y_{\mu,i,j}(k_m) \Xi_{j,z}(v_{\mu,i}(k_m)) v_{\mu,i,j}(k_m) T_m \quad (57)$$

where it is explicitly assumed that all vehicles in the segment have the same speed. For origin links, the same quantity is given from

$$E_{o,j,z}(k_m) = w_o(k_m) \Xi_{j,z}(\hat{v}_o(k_m)) \hat{v}_o(k_m) T_m \quad (58)$$

where $\hat{v}_o(k_m)$ is an estimate of the mean speed in origin link o . It is set to 10 km/h, which is the lower bound of validity of the COPERT models (Ntziachristos and Kouridis, 2007).

4.2. Global and local environmental policies

Global policies are based on the total quantity of pollutant z emitted in a network from all vehicle classes $E_{z,total}(k_m)$ (grams) during time period k_m , where

$$E_{z,total}(k_m) = \sum_{\mu \in \mathcal{S}_M} \sum_{i=1}^{S_\mu} \sum_{j \in \mathcal{J}} E_{\mu,i,j,z}(k_m) + \sum_{o \in \mathcal{S}_O} \sum_{j \in \mathcal{J}} E_{o,j,z}(k_m). \quad (59)$$

As mentioned in Section 2, minimising $\sum_{k_m} E_{z,total}(k_m)$ is a blanket policy encompassing the whole network without paying attention to SIA. Let \mathcal{A} denote the index set of SIA in the network and η its index. A special interest area $\mathcal{A}_\eta \in \mathcal{A}$ is itself a set of motorway segments and origin links outlining the area of interest and a pair of model time step indices $(k_\eta^{(1)}, k_\eta^{(2)})$, which define the time period where local environmental rules are applied.

Let $E_z^{(\mathcal{A}_\eta)}(k_\eta^{(1)}, k_\eta^{(2)})$ (grams) be the total amount of emissions of pollutant z from time step $k_\eta^{(1)}$ to $k_\eta^{(2)}$ in area η , which should not be larger than a maximum quantity $E_{z,max}^{(\mathcal{A}_\eta)}$ (grams). The same area may have a different maximum for another time interval, as regulations dictate. This type of regulatory requirements yield the constraints

$$E_z^{(\mathcal{A}_\eta)}(k_\eta^{(1)}, k_\eta^{(2)}) = T_m \sum_{j \in \mathcal{J}} \sum_{k_m=k_\eta^{(1)}}^{k_\eta^{(2)}} \left\{ \sum_{(\mu,i) \in \mathcal{A}_\eta} \Delta_\mu l_\mu y_{\mu,i,j}(k_m) \Xi_{j,z}(v_{\mu,i}(k_m)) v_{\mu,i,j}(k_m) + \sum_{o \in \mathcal{A}_\eta} y_{o,j}(k_m) \Xi_{j,z}(\hat{v}_o(k_m)) \hat{v}_o(k_m) \right\} \leq E_{z,max}^{(\mathcal{A}_\eta)}. \quad (60)$$

Another constraint can be imposed on the rate of emissions. Let $G_z^{(\mathcal{A}_\eta)}(k_m)$ (grams/h) be the emission rate of pollutant z during k_m , which should be less than a predetermined threshold $G_{z,max}^{(\mathcal{A}_\eta)}(k_m)$ (grams/h) for the period of interest, i.e.

$$G_z^{(\mathcal{A}_\eta)}(k_m) = \sum_{j \in \mathcal{J}} \left\{ \sum_{(\mu,i) \in \mathcal{A}_\eta} \Delta_\mu l_\mu y_{\mu,i,j}(k_m) \Xi_{j,z}(v_{\mu,i}(k_m)) v_{\mu,i,j}(k_m) + \sum_{o \in \mathcal{A}_\eta} y_{o,j}(k_m) \Xi_{j,z}(\hat{v}_o(k_m)) \hat{v}_o(k_m) \right\} \leq G_{z,max}^{(\mathcal{A}_\eta)}(k_m), k_\eta^{(1)} \leq k_m \leq k_\eta^{(2)}. \quad (61)$$

The rationale behind constraints (60) is to impose limits on the pollutant mass accumulated during a certain period. Constraint (60) is insensitive to the distribution of the total mass released over space and time. Imposing limits on this distribution is achieved with constraints (61) limiting the rate of emissions. The parametrisation of these constraints allows for the gradual easing and tightening of restrictions by varying $G_{z,max}^{(\mathcal{A}_\eta)}(k_m)$ over time for (61) and by defining different SIA with the same location but different $k_\eta^{(1)}, k_\eta^{(2)}$ and $E_{z,max}^{(\mathcal{A}_\eta)}$ for (60).

5. Optimal control problem formulation

The general discrete time optimal control problem has the form

$$\min_{\mathbf{r}} \Lambda = \sum_{k_m=0}^{K_m-1} \lambda[\mathbf{x}(k_m), \mathbf{r}(k_m), \mathbf{d}(k_m); \mathbf{p}(k_m)] + \varphi[\mathbf{x}(k_m)] \quad (62)$$

subject to

$$\mathbf{x}(k_m + 1) = \mathbf{f}[\mathbf{x}(k_m), \mathbf{r}(k_m), \mathbf{d}(k_m); \mathbf{p}(k_m)] \quad (63)$$

$$\mathbf{\Pi}[\mathbf{x}(k_m), \mathbf{r}(k_m), \mathbf{d}(k_m); \mathbf{p}(k_m)] \geq \mathbf{0} \quad (64)$$

$$\mathbf{r}_{\min} \leq \mathbf{r}(k_m) \leq \mathbf{1} \quad (65)$$

where \mathbf{x} is the state vector, \mathbf{r} the control vector, \mathbf{d} the disturbance vector, \mathbf{p} the model parameters vector, Λ the total cost criterion, λ a state transition cost functional, φ a final state cost, \mathbf{f} the system model, $\mathbf{\Pi}$ a vector of state and control dependent problem constraints and \mathbf{r}_{\min} the lower bounds of the control variables, with $\mathbf{1}$ been set as their default upper bound.

The traffic model state vector is $\mathbf{x}_m = [\dots \rho_{\mu,i} v_{\mu,i} y_{\mu,i,1} \dots y_{\mu,i,|\mathcal{J}|} \dots w_o y_{o,1} \dots y_{o,|\mathcal{J}|} \dots]^T$. The control vector \mathbf{r} consists of the RM rates of the controlled on-ramps and has the form $\mathbf{r} = [\dots r_o \dots]^T, o \in \mathcal{L}_O$. The disturbance vector \mathbf{d} consists of the demand and its composition at every origin link, the turning rates at every bifurcation and has the form $\mathbf{d} = [\dots d_o \theta_{o,1} \dots \theta_{o,|\mathcal{J}|} \dots \beta_{n,\mu} \dots]^T, o \in \mathcal{L}_O, n \in \mathcal{N}$. The right hand sides of the dynamic equations of the mean speed, total and partial densities and queues constitute \mathbf{f}_m . $\mathbf{\Pi}$ contains the special areas environmental emissions constraints (60) and (61).

(60) are inter-temporal constraints that can be treated by introducing additional state variables $x_{\mathcal{A}_\eta, z}(k_m)$ (grams) representing the cumulative emissions of pollutant z in area \mathcal{A}_η until time period k_m . Their state equations are

$$x_{\mathcal{A}_\eta, z}(k_m + 1) = \begin{cases} x_{\mathcal{A}_\eta, z}(k_m) = 0 & \text{if } k_m < k_\eta^{(1)} \\ E_z^{(\mathcal{A}_\eta)}(k_m, k_m) + x_{\mathcal{A}_\eta, z}(k_m) & \text{if } k_\eta^{(1)} \leq k_m \leq k_\eta^{(2)} \\ x_{\mathcal{A}_\eta, z}(k_m) & \text{if } k_m > k_\eta^{(2)}. \end{cases} \quad (66)$$

The cumulative emissions state variables vector $\mathbf{x}_{\mathcal{A}}$ has the form $\mathbf{x}_{\mathcal{A}} = [\dots x_{\mathcal{A}_1,1} \dots x_{\mathcal{A}_1,|\mathcal{Z}|} \dots]^T, \eta \in \mathcal{A}$ yielding the total state vector $\mathbf{x} = [\mathbf{x}_m^T \mathbf{x}_{\mathcal{A}}^T]^T$. The SIA emissions model $\mathbf{f}_{\mathcal{A}}$ consists of the right hand sides of the $|\mathcal{Z}||\mathcal{A}|$ Eqns. (66). The total system model is $\mathbf{f} = [\mathbf{f}_m^T \mathbf{f}_{\mathcal{A}}^T]^T$. Similarly, the parameters of (60) and (61) are organised into vector $\mathbf{p}_{\mathcal{A}}$ yielding the full parameter vector $\mathbf{p} = [\mathbf{p}_m^T \mathbf{p}_{\mathcal{A}}^T]^T$.

Constraints (60) are considered by the final state cost functional φ , which takes the form

$$\varphi[\mathbf{x}(k_m)] = \sum_{\eta \in \mathcal{A}} \sum_{z \in \mathcal{Z}} \omega_{z,term} \max \left\{ 0, x_{\mathcal{A}_\eta, z}(k_m) - E_{z,max}^{(\mathcal{A}_\eta)} \right\}^2 \quad (67)$$

where $\omega_{z,term}$ weighting parameters. The part of (64) corresponding to constraints (60) are replaced by the state Eqs. (66) in conjunction with (67). The remaining parts of constraints (64) corresponding to constraints (61) are implicitly considered by introducing the penalty terms λ_{maxe} in λ , given from

$$\lambda_{maxe}[\mathbf{x}(k_m), \mathbf{r}(k_m), \mathbf{d}(k_m); \mathbf{p}(k_m)] = \sum_{\eta \in \mathcal{A}} \sum_{z \in \mathcal{Z}} \max \left\{ 0, G_z^{(\mathcal{A}_\eta)}(k_m) - G_{z,max}^{(\mathcal{A}_\eta)} \right\}^2. \quad (68)$$

This allows for (64) to be dropped from the problem formulation.

The other main elements of the cost functional λ are the network wide traffic efficiency, equity, queue constraints and emissions metrics. Traffic efficiency is measured by the TTS λ_{TTS} (veh-h) by all vehicles in the network travelling in the motorways and queueing at the origins during period k_m given from

$$\lambda_{TTS}[\mathbf{x}(k_m), \mathbf{r}(k_m), \mathbf{d}(k_m); \mathbf{p}(k_m)] = T_m \left[\sum_{\mu \in \mathcal{I}_R} \sum_{i=1}^{S_\mu} \Delta_\mu l_\mu \rho_{\mu,i}(k_m) + \sum_{o \in \mathcal{L}_O} w_o(k_m) \right]. \quad (69)$$

Equity can be considered either explicitly or implicitly. The explicit equity expression is a measure of the variance over the on-ramps of the average time it takes a vehicle to wait in the queue to get to the motorway plus the average time it takes to travel through a representative length of motorway, (Kotsialos and Papageorgiou, 2004a). Let Δ_{eq} (km) denote this representative distance and let $\mathcal{L}_o^{(eq)}$ denote the set of links immediately downstream of o for which $\sum_{\mu \in \mathcal{L}_o^{(eq)}} \Delta_\mu \approx \Delta_{eq}$. Then the mean travel and queuing time for origin o during period k_m is given from

$$t_o^{(eq)}(k_m) = \frac{w_o(k_m)}{q_o(k_m)} + \sum_{\mu \in \mathcal{L}_o^{(eq)}} \sum_{i=1}^{S_\mu} \frac{\Delta_\mu}{v_{\mu,i}(k_m)} \quad (70)$$

and its mean over the network on-ramps from

$$\bar{t}^{(eq)}(k_m) = \frac{1}{|\mathcal{L}_o|} \sum_{o \in \mathcal{L}_o} t_o^{(eq)}(k_m). \quad (71)$$

Equity is a measure of the variance of the mean travel times over the network's on-ramps λ_{equi} (h^2) given from

$$\lambda_{equi}[\mathbf{x}(k_m), \mathbf{r}(k_m), \mathbf{d}(k_m); \mathbf{p}(k_m)] = \frac{1}{|\mathcal{L}_o|} \sum_{o \in \mathcal{L}_o} [\bar{t}^{(eq)}(k_m) - t_o^{(eq)}(k_m)]^2. \quad (72)$$

Equity is implicitly considered by the introduction of maximum queues at each origin $o, w_{o,\max}$ (veh). Deviation penalty terms are introduced to λ and their contribution are given from

$$\lambda_{maxq}[\mathbf{x}(k_m), \mathbf{r}(k_m), \mathbf{d}(k_m); \mathbf{p}(k_m)] = \sum_{o \in \mathcal{L}_o} \max\{0, w_o(k_m) - w_{o,\max}\}^2. \quad (73)$$

The CRM strategy considers the total weighted hot gas emissions by including the following term in λ

$$\lambda_{toem}[\mathbf{x}(k_m), \mathbf{r}(k_m), \mathbf{d}(k_m); \mathbf{p}(k_m)] = \sum_{z \in \mathcal{Z}} \omega_{z,tot} E_{z,total}(k_m) \quad (74)$$

where $\omega_{z,tot}$ weights representing the importance of each pollutant and the scale of the output of the emissions model.

Finally, because there is a preference towards trajectories $r_o(k_c)$ that do not change rapidly in two successive control periods the following penalty terms are included in λ

$$\lambda_{rvvar}[\mathbf{x}(k_m), \mathbf{r}(k_m), \mathbf{d}(k_m); \mathbf{p}(k_m)] = \sum_{o \in \mathcal{L}_o} [r_o(k_m - 1) - r_o(k_m)]^2. \quad (75)$$

Now, λ is a weighted sum of contributions (68), (69) and (72)–(75), i.e.

$$\lambda = \omega_0 \lambda_{TTS} + \omega_1 \lambda_{equi} + \omega_2 \lambda_{maxq} + \omega_3 \lambda_{rvvar} + \omega_4 \lambda_{toem} + \omega_5 \lambda_{max} \quad (76)$$

where $\omega_0, \dots, \omega_5$ are weighting parameters set manually.

The resulting optimal control problem can be solved by a host of algorithms. The most efficient ones are gradient based coupled with a globalisation method, (Kotsialos, 2019; Poole and Kotsialos, 2016a). These algorithms require the analytical expression of $\partial f / \partial \mathbf{x}$ for obtaining the gradient vector of the resulting large scale static nonlinear optimisation problem, (Kotsialos et al., 2002b; Kotsialos and Papageorgiou, 2004c). In view of the speed equation parameter dependence on the extended system state, this is a fairly complicated task. Developing such an algorithm is a challenging problem and requires substantial effort, beyond the scope of this paper. Instead, the Differential Evolution (DE) (Storn and Price, 1997) search algorithm is used as a simple but efficient evolutionary algorithm.

6. Differential evolution and solution evaluation

6.1. The differential evolution algorithm

Evolutionary algorithms have been applied to various optimal control problems that occur in practice, (Fleming and Purshouse, 2002; Cruz, 2002). A recent review for their application to traffic control problems can be found in (Shaikh et al., 2020) and in (Pasquale et al., 2016a) a comparison of gradient based and stochastic search algorithms for the two-class RM problem is given. DE (Storn and Price, 1997) is a highly efficient evolutionary search algorithm, applied successfully to various problems (Chakraborty, 2008), including unconventional computing where gradient information is impossible to calculate, (Vissol-Gaudin et al., 2017).

The approach followed for solving the optimal control problem is that of (Kotsialos et al., 2002b; Kotsialos and Papageorgiou, 2004c), where the dynamic optimisation control problem is turned into a large-scale static one. By starting from a known initial state \mathbf{x}_0 and given the disturbance trajectory \mathbf{d} , the state $\mathbf{x}(k_m)$ produced by the forward integration of (63) becomes a function of $\mathbf{r}(k_m)$ and in view of (54) of $\mathbf{r}(k_c)$. Embedding (63) into the cost criterion Λ results to a function that depends on $\mathbf{r}(k_c)$. The independent variables of

this problem are the ramp metering rates $r_o(k_c)$ for every metered origin link o at every control time step k_c . In a network where all origin links are under control, there are $|\mathcal{L}_O| \lfloor \frac{K_m}{\alpha_{cm}} \rfloor$ decision variables. Given $\mathbf{r}(k_m)$ and the resulting trajectories $\mathbf{x}(k_m)$ from the forward integration of (63), the evaluation of (76) for every time step k_m and of (67) at step K_m allow the calculation of objective function (62) as $\Lambda(\mathbf{r}(0), \dots, \mathbf{r}(k_m), \dots, \mathbf{r}(K_m - 1))$.

DE uses a number P_{DE} of individuals, or agents, each with its own set of vectors $\mathbf{r}_\zeta(k_m)$, $k_m = 0, \dots, K_m - 1, \zeta = 1, \dots, P_{DE}$ and corresponding objective function value Λ_ζ . The search algorithm executes ℓ_{\max} iterations and stops earlier if ℓ_1 iterations have passed without improving the current best solution. A scaling factor f_{DE} is used for the differences in the mutation operation and a crossover rate c_{DE} . All three parameters are pre-set manually. The stochastic search algorithm has the following form.

Algorithm 1. differential evolution for coordinated ramp metering

```
(*DE iteration loop*)
Input: model f, initial state  $\mathbf{x}_0$ , emissions model parameters  $\xi$ , weights  $\omega, \mathbf{r}_{\min}, P_{DE}, c_{DE}, f_{DE}, \ell_{\max}, \ell_1$ 
Output: optimal ramp metering rates trajectories  $r_o^*(k_m), \forall o \in \mathcal{L}_O, k_m = 0, \dots, K_m - 1$ 

1: randomly select  $r_{\zeta,o}^{(0)}(k_c) \sim U(r_{\min}, 1), \zeta = 1, \dots, P_{DE}, o = 1, \dots, |\mathcal{L}_O|, k_c = 0, \dots, \frac{K_m}{\alpha_{cm}} - 1$ 
2: for  $\zeta = 1$  to  $P_{DE}$  do
3:   evaluate  $\Lambda_\zeta^{(0)}$ 
4:    $\zeta^* \leftarrow \text{argmin}_\zeta \Lambda^{(0)}$ 
5:    $\mathbf{r}^* \leftarrow \mathbf{r}_{\zeta^*}, \Lambda^* \leftarrow \Lambda_{\zeta^*}$ 
6:    $\ell \leftarrow 1$ 
7:    $\tilde{\ell} \leftarrow 0$ 
8: repeat
9:   for  $\zeta = 1$  to  $P_{DE}$ 
10:  select randomly integers  $\zeta_1, \zeta_2, \zeta_3 \in \{1, \dots, P_{DE}\}$  with  $\zeta_1 \neq \zeta, \zeta_2 \neq \zeta$  and  $\zeta_3 \neq \zeta$ 
11:  select randomly integer  $R \in \left\{1, \dots, |\mathcal{L}_O| \binom{K_m}{\alpha_{cm}}\right\}$ 
12:  for  $j = 1$  to  $|\mathcal{L}_O| \binom{K_m}{\alpha_{cm}}$ 
13:     $o \leftarrow \lfloor \frac{j}{\frac{K_m}{\alpha_{cm}}} \rfloor$ 
14:     $k_c \leftarrow j - o \frac{K_m}{\alpha_{cm}}$ 
15:    select randomly  $u \sim U(0, 1)$ 
16:    if  $(j = R \vee u < c_{DE})$ 
17:      if  $\zeta < \frac{P_{DE}}{2}$ 
18:         $\tilde{r}_o(k_c) \leftarrow r_{\zeta_1,o}(k_c)^{(\ell-1)} + f_{DE} \left( r_{\zeta_2,o}(k_c)^{(\ell-1)} - r_{\zeta_3,o}(k_c)^{(\ell-1)} \right)$ 
19:        if  $\zeta \geq \frac{P_{DE}}{2}$ 
20:           $\tilde{r}_o(k_c) \leftarrow r_{\zeta,o}(k_c)^{(\ell-1)} + f_{DE} \left( r_{\zeta_1,o}(k_c)^{(\ell-1)} - r_{\zeta_3,o}(k_c)^{(\ell-1)} \right)$ 
21:           $\tilde{r}_o(k_c) \leftarrow \tilde{r}_o(k_c) + f_{DE} \left( r_{\zeta_2,o}(k_c)^{(\ell-1)} - r_{\zeta_3,o}(k_c)^{(\ell-1)} \right)$ 
22:        if  $\tilde{r}_o(k_c) < r_{\min}$ 
23:           $\tilde{r}_o(k_c) \leftarrow r_{\min}$ 
24:        if  $\tilde{r}_o(k_c) > 1$ 
25:           $\tilde{r}_o(k_c) \leftarrow 1$ 
26:        else
27:           $\tilde{r}_o(k_c) \leftarrow r_{\zeta,o}(k_c)^{(\ell-1)}$ 
28:        evaluate  $\Lambda(\tilde{r}_o(k_c))$ 
29:         $\tilde{\Lambda} \leftarrow \Lambda(\tilde{r}_o(k_c))$ 
30:        if  $\tilde{\Lambda} < \Lambda_\zeta^{(\ell-1)}$ 
31:           $\mathbf{r}_\zeta^{(\ell)} \leftarrow \tilde{\mathbf{r}}, \Lambda_\zeta^{(\ell)} \leftarrow \tilde{\Lambda}$ 
32:          if  $\Lambda_\zeta^{(\ell)} < \Lambda^*$ 
33:             $\zeta^* \leftarrow \zeta, \mathbf{r}^* \leftarrow \mathbf{r}_\zeta^{(\ell)}, \Lambda^* \leftarrow \Lambda_\zeta^{(\ell)}, \tilde{\ell} \leftarrow 0$ 
34:            if  $\tilde{\Lambda} \geq \Lambda_\zeta^{(\ell-1)}$ 
35:               $\mathbf{z}_\zeta^{(\ell)} \leftarrow \mathbf{z}_\zeta^{(\ell-1)}, \Lambda_\zeta^{(\ell)} \leftarrow \Lambda_\zeta^{(\ell-1)}$ 
36:               $\ell \leftarrow \ell + 1$ 
37:             $\tilde{\ell} \leftarrow \tilde{\ell} + 1$ 
38: until  $(\ell = \ell_{\max} \vee \tilde{\ell} > \ell_1)$ 
```

Lines 17 and 18 implement a DE/rand/1 mutation operation for half the population, whereas lines 19–21 a DE/rand-to-best/1 for the other half, (Qin et al., 2009), since numerical experience has shown that this scheme has better convergence properties.

6.2. Performance evaluation metrics

A number of different scenarios are considered and for each of them a set of experiments is conducted. The outcome of each experiment is evaluated against a number of metrics. The metrics covering efficiency are the TTS and TWT, $\Phi_{TTS,tot}$ and $\Phi_{TWT,tot}$, respectively given by

$$\Phi_{TTS,tot} = \sum_{k_m=0}^{K_m} \lambda_{TTS}[\mathbf{x}(k_m), \mathbf{r}(k_m), \mathbf{d}(k_m); \mathbf{p}(k_m)] \quad (77)$$

$$\Phi_{TWT,tot} = T_m \sum_{k_m=0}^{K_m} \sum_{o \in \mathcal{O}} w_o(k_m). \quad (78)$$

Equity is assessed by the time averaged variance $\lambda_{equi,tot}$ given by

$$\Phi_{equi,tot} = \frac{1}{K_m} \sum_{k_m=0}^{K_m-1} \lambda_{equi}[\mathbf{x}(k_m), \mathbf{r}(k_m), \mathbf{d}(k_m); \mathbf{p}(k_m)]. \quad (79)$$

The network wide emissions of each particular pollutant $z \in \mathcal{Z}, \lambda_{z,tot}$ are used as metrics, given from

$$\Phi_{z,tot} = \sum_{k_m=0}^{K_m} E_{z,total}(k_m), z \in \mathcal{Z}. \quad (80)$$

The SIA environmental metrics with respect to constraints (60) are the total emitted quantity of each pollutant during the corresponding time period of interest given from

$$\Phi_{term}^{(\eta,z)} = x_{\mathcal{A}_{\eta,z}}(k_m), z \in \mathcal{Z}, \eta \in \mathcal{A}. \quad (81)$$

With respect to constraint (61), the following performance index is calculated for each SIA η and pollutant z

$$\Phi_{max}^{(\eta,z)} = \sqrt{\sum_{k_m=0}^{K_m-1} \max \left\{ 0, G_z^{(\mathcal{A}_\eta)}(k_m) - G_{z,max}^{(\mathcal{A}_\eta)} \right\}^2}. \quad (82)$$

The means and the standard deviations of the Φ metrics are estimated from repeated experiments for each scenario. The same parameters of the stochastic search performed by the DE are used with different randomised starting points and random number generator seeds. The results are also compared to those obtained from a single run of the DE with more maximum number of iterations allowed and larger population size. This approach is followed in the next section, where a small case study is discussed.

7. Test network case study

7.1. Site description

In order to demonstrate the model developed and the CRM solutions, the test network shown in Fig. 7 was designed. It consists of two parallel motorways, Route 1 and Route 2 connected by motorway-to-motorway links at junctions MJ1 and MJ2. The motorway links' length and number of lanes are displayed. Route 1 is 9.5 km long and Route 2 9.8 km. Each has two on-ramps and two off-ramps attached at their sides with the main origin at the leftmost upstream point and the main destination at the rightmost downstream point. The dashed outlines of two SIAs, SIA 1 and SIA 2, are shown as well.

Traffic consists of five different vehicle classes, Euro1 to Euro4 petrol (gasoline) pc and Euro3 diesel trucks at 50% load. Thus, $\mathcal{J} = \{1, 2, 3, 4, 5\}$ yielding, $\mathcal{J}_{pc} = \{1, 2, 3, 4\}$ and $\mathcal{J}_{tr} = \{5\}$. The model parameters lower and upper values are given in Table 2. For pc $g_{max,j}$ is 37,195.2 km/h² and $g_{min,j}$ is 56,116.8 km/h², $j \in \mathcal{J}_{pc}$, whereas for trucks the corresponding quantities are 12,960 km/h² and 11,404.8 km/h². Based on (35) the model time step is set $T_m = 0.00098$ h or 3.53 s. The simulation horizon is 3.5 h or 3,571 model time

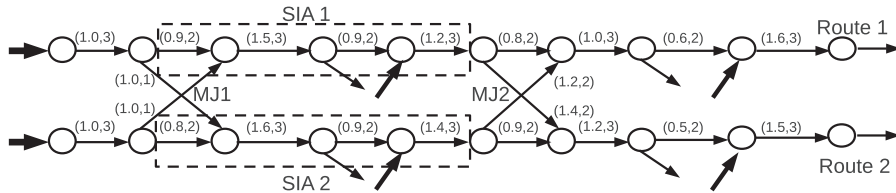


Fig. 7. Test network topology and Special Interest Areas. In parenthesis the links' length and number of lanes ($\Delta_\mu S_\mu, l_\mu$). Thicker arrows denote origin links.

Table 2

Parameter lower and upper bounds for the case study as functions of composition rates.

$p_{\varsigma}^{(1)}$	$p_{\varsigma}^{(2)}$	(units)
$\rho_{\varsigma,cr}(0,1) = 23.2$	$\rho_{\varsigma,cr}(1,0) = 33.2$	(veh/km/lane)
$a_{\varsigma}(1,0) = 2.3$	$a_{\varsigma}(0,1) = 3.8$	(–)
$v_{\varsigma,max}(0,1) = 80$	$v_{\varsigma,max}(1,0) = 110$	(km/h)
$\tau_{\varsigma}(1,0) = 0.0024$	$\tau_{\varsigma}(0,1) = 0.0073$	(h)
$\nu_{\varsigma}(1,0) = 14$	$\nu_{\varsigma}(0,1) = 44$	km^2/h
$\delta_{\varsigma}(1,0) = 28E-7$	$\delta_{\varsigma}(0,1) = 48E-7$	(–)
$\phi_{\varsigma}(1,0) = 28E-5$	$\phi_{\varsigma}(0,1) = 48E-5$	(–)
$Q_{\varsigma,max}(0,1) = 6,500$	$Q_{\varsigma,max}(1,0) = 8,500$	(veh/h) main entrances
$Q_{\varsigma,max}(0,1) = 1,000$	$Q_{\varsigma,max}(1,0) = 1,800$	(veh/h) on-ramps

steps. For the multi-class model, the triplet $(\psi_1, \psi_2^{(0)}, \psi_3) = (18, 0.7, 4)$ is used for all traffic model parameters. This simplification is used for illustration purposes, since different triplets are expected to be identified for different parameters from a model validation exercise.

The demand and its composition generated at each origin along both routes can be seen in Fig. 8. Each subfigure displays the sum of *pc* and truck demands and the trucks' part of it. Route 1 main entrance has a significantly higher truck demand than Route 2's, but still the bulk of traffic volume consists of *pc*. The first on-ramp of Route 1 carries mostly truck demand and some *pc*, whereas the second on-ramp has much lower truck demand. The reverse situation takes place in Route 2, where it is the demand at the second on-ramp that consists mainly from trucks.

Fig. 8(g) and (h) provide the turning rates junctions at MJ1, MJ2 and off-ramps. The trajectories shown refer to the traffic volume continuing their trip along the main direction of travel. The turning rates vary over time during the peak hour and settle to constant levels afterwards. The turning rate of Route 1 towards Route 2 at MJ2, shows a strong preference of Route 1 traffic diverting towards Route 2.

7.2. The no-control case

Fig. 9 shows the density spatio-temporal profiles and queues formed at Routes 1 and 2 in the absence of any control measures. Congestion in Route 1 is formed in the area between the first on-ramp and MJ2 and is amplified by the increased demand at the main entrance. The increased truck demand of the first on-ramp merging with the mainstream flow has a stronger negative impact on the mean speed in that area. The increased truck flow from Route 1 to Route 2 at MJ2 is the cause for the shockwaves originating towards the downstream end of Route 2 (subfigure (c)). This congestion spills back into Route 1 via MJ2 and combined with the outflow from the first on-ramp, causes the congestion in Route 1. The density peak observed in Route 1 around km 3 between time steps 1,500 and 2,500 (sub Fig. 9(a)) is a stationary shockwave formed by the drop in the number of lanes, from 3 to 2, at km 3.4, directly upstream the first off-ramp.

The congestion formed in Route 2 at MJ2 propagates upstream and extents just past its first off-ramp and before the motorway connector from Route 1 to Route 2 of MJ1. Density is at a lower level at the area between the main entrance and the first off-ramp compared to the area downstream. This is reflected on the queues of subfigure (d), where no queue is formed at Route 2 main origin but only at the two on-ramps. The queues of Route 1, shown in subfigure (b), propagate back into the main entrance, highlighting the fact that Route 1 is busier than Route 2.

Fig. 10 provides an additional piece of information, which is a spatio-temporal profile of the critical density as it changes with the composition of traffic along Routes 1 and 2. In single-class models these surfaces are considered as flat. The more detailed representation of traffic provided by the multi-class model allows tracking the evolution of the model parameters over time.

Fig. 11 provides the detailed CO emissions heatmaps, in (grams/h), for each vehicle class at (a)–(e) and the total CO emissions in (f), for Route 1. The contribution of older technology Euro1 *pc* is distinctive, but clearly the main contributors are the trucks. Fig. 12 displays the CO and NO_x emissions at the on-ramps of Route 1 at (a) and (b), respectively. Fig. 13 displays the NO_x heatmap of emissions for Route 1 from truck traffic at (a) and the total emissions at (b). The heatmaps of the individual *pc* class contributions are insensitive to the scale and appear as flat profiles, hence, in the interest of brevity, they are omitted. The main contributors of hot NO_x emissions are trucks (Fig. 14). The corresponding emissions for Route 2 are given in Figs. 15 and 16.

Against this background, the TTS is 6,492.01 veh·h and the Total Waiting Time (TWT) part of it is 2,229.45 veh·h. The equity index is calculated for each origin and about 2 km downstream in the motorway, as shown in Table 3, and $\Phi_{equi,tot} = 0.031505 \text{ h}^2$. The total network-wide CO emissions are 246,973.56 grams and of NO_x are 216,781.28 grams.

The special interest areas SIA 1 and 2 shown in Fig. 7 are 4.5 km and 4.7 km, respectively, long. Both extent from the bifurcations of MJ1 and end about 1.3 km past the first on-ramp of their respective Route. The time intervals for constraints (60) are set from time step 300 to time step 2,341 for SIA 1, i.e. about 2 h, and for SIA 2 from time step 300 to time step 2,851, i.e. about 2.5 h. For both cases, the total mass of CO and NO_x emitted during these periods should not exceed 8,000 grams for each pollutant. Thus, for SIA 1 the average desired hourly rates of CO and NO_x emissions is about 4,000 grams/h and for SIA 2 about 3,200 grams/h for both pollutants. In the no-control case, the CO cumulative emissions during the period of interest for SIA 1 are 52,430.09 grams and for NO_x 89,554.21 grams.

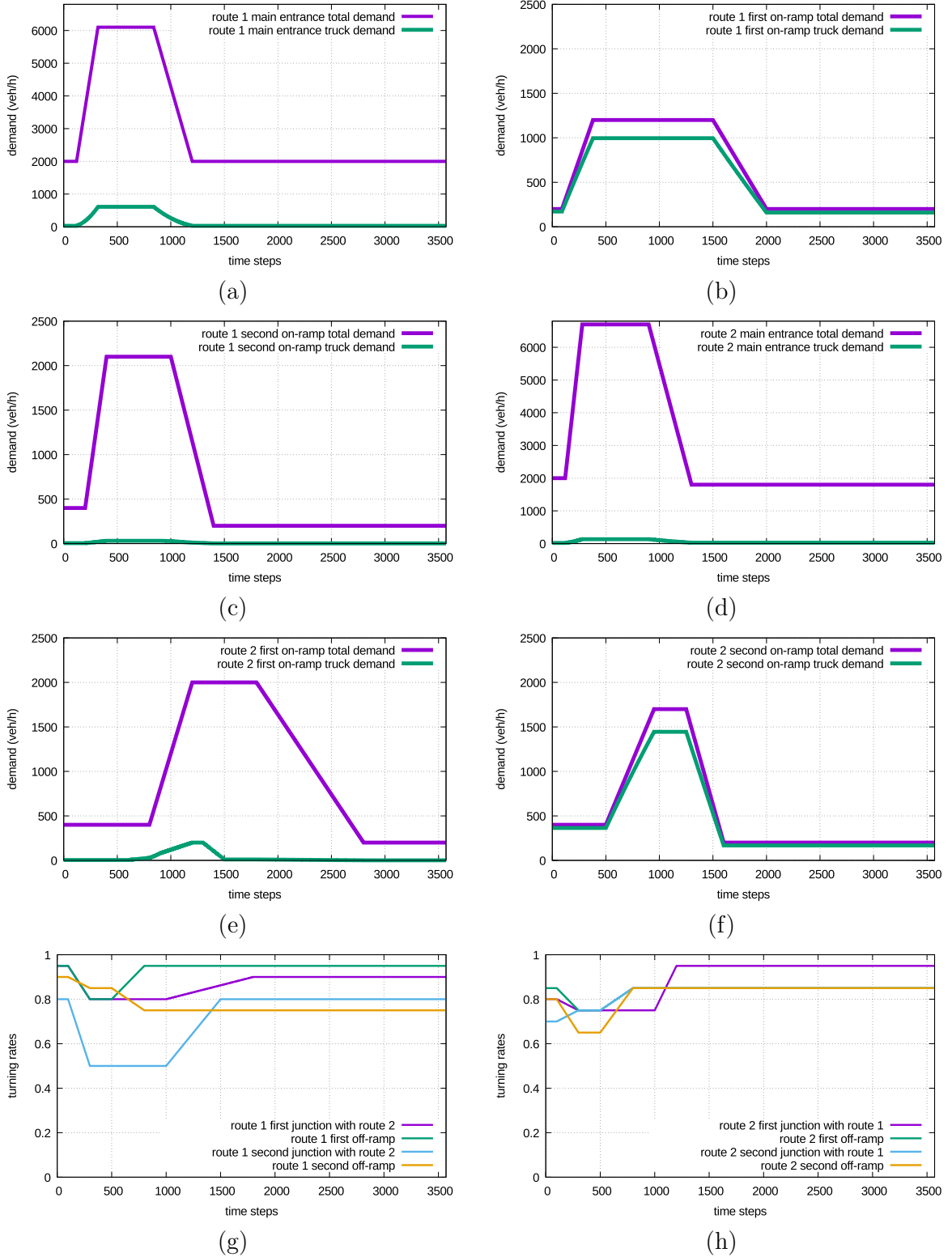


Fig. 8. System disturbance trajectories. Total demand and truck demand profiles for each on-ramp: Route 1 (a) main entrance, (b) 1st on-ramp, (c) 2nd on-ramp. Route 2 (d) main entrance, (e) 1st on-ramp, (f) 2nd on-ramp; turning rates along the main direction of travel: (g) Route 1, (h) Route 2.

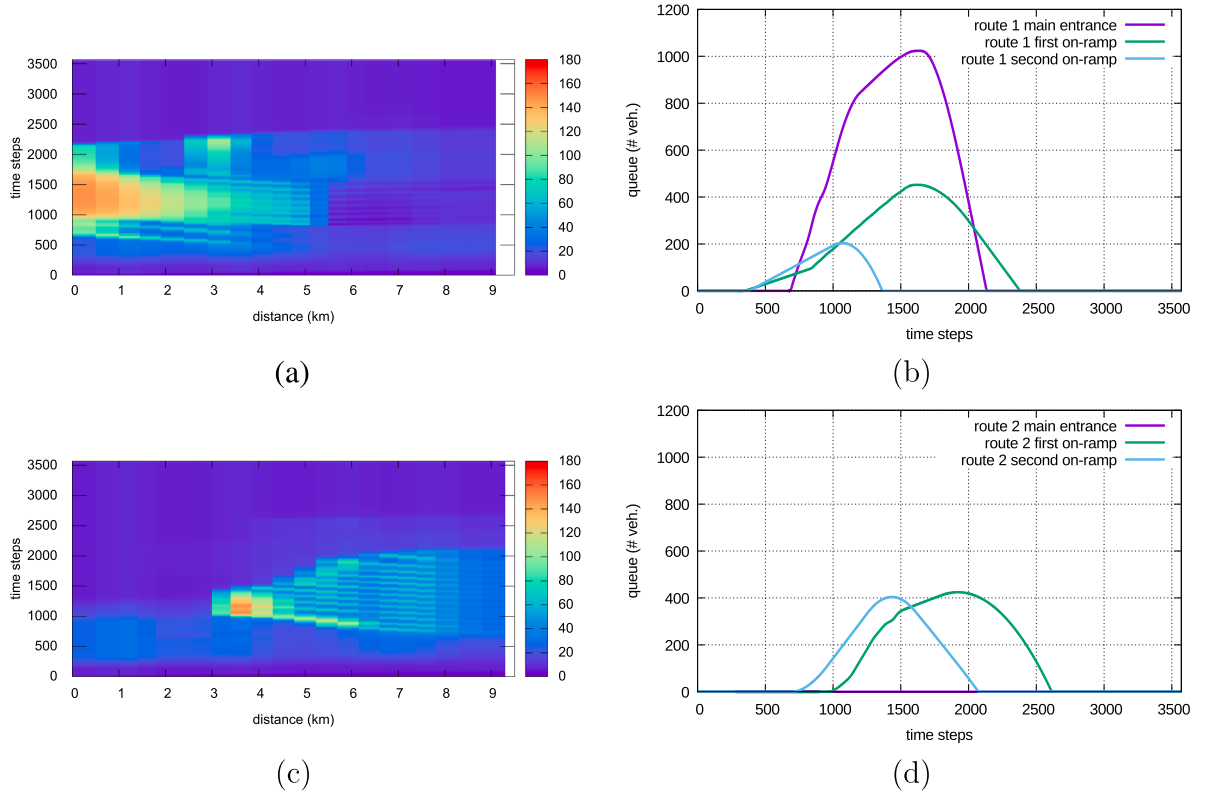


Fig. 9. No-control density and queue spatio-temporal profiles. (a), (b) Route 1. (c), (d) Route 2.

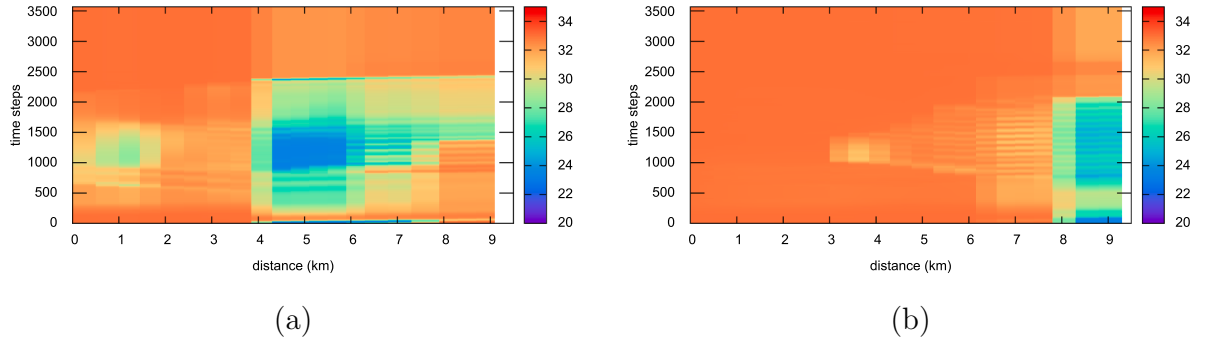


Fig. 10. No-control critical density profiles. (a) Route 1. (b) Route 2.

The corresponding numbers for SIA 2 are 39,350.32 grams CO and 18,153.24 grams NO_x . In other words, SIA 1 receives 21.0% and 41.6% of CO and NO_x , respectively, of network emissions over the whole time horizon and SIA 2 the 16.0% and 8.4%, respectively. These results highlight the fact that Route 1 carries a larger percentage of truck traffic and is more heavily used as well as the fact that truck traffic in Route 2 is heavier at the downstream section of the road, rather than upstream. Combined, the two SIA receive about 37% of the CO and about 50% of the NO_x total network emissions.

For constraints given from (61), the period of interest for both SIA is from time step 225 to 450, i.e. a short period of about 13 min. During this period the rate of pollutant transmission is set for the first 900 metres of SIA 1 to 1,700 grams/h for both CO and NO_x and then for the rest 3.6 km the thresholds are set to 1,800 grams/h. For SIA 2, all thresholds are set to 1,800 grams/h. Furthermore, for the on-ramps in each SIA, the thresholds for CO and NO_x are set to 10,000 grams/h and 40,000 gram/h, respectively.

7.3. Ramp metering scenarios

Eight scenarios customizing the CRM strategy of Section 5 are visited, with scenario 0 been the no-control case. Scenario 1, is the maximum efficiency case without queue nor environmental constraints and no concern for equity, with minimisation of the TTS as the

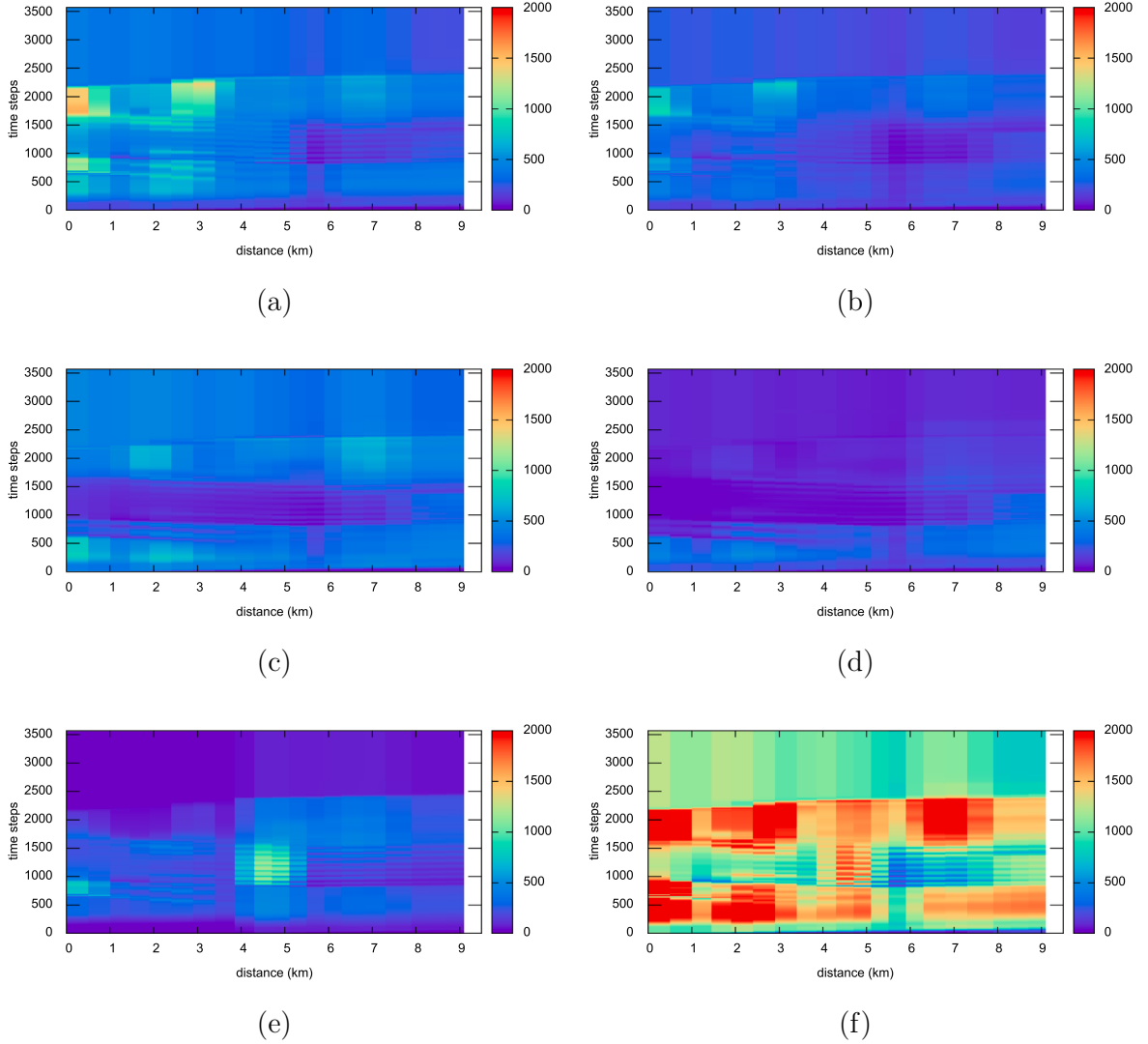


Fig. 11. No-control CO emissions (grams/h) along Route 1 motorway links (grams/hour) due to: (a) Euro1 pc, (b) Euro2 pc, (c) Euro3 pc, (d) Euro4 pc, (e) Euro3 diesel trucks and (f) total CO emissions.

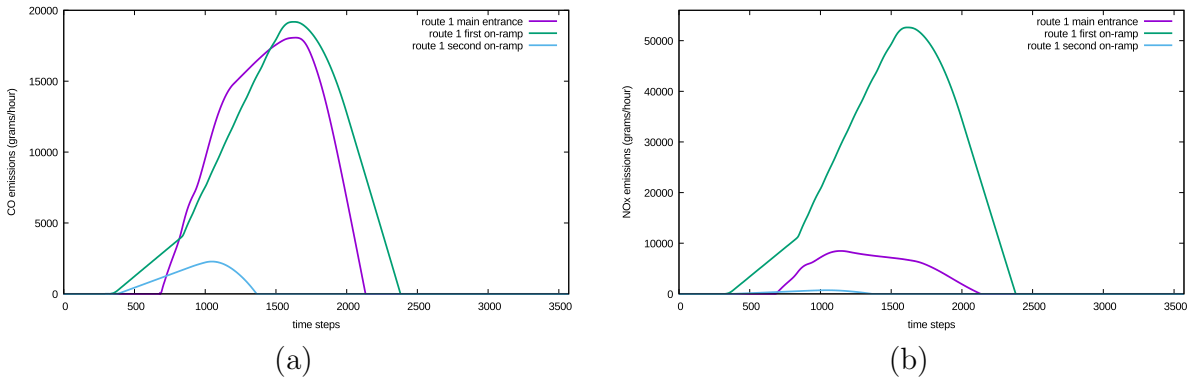


Fig. 12. No-control Route 1 total emissions at on-ramps. (a) CO (grams/hour), (b) NOx (grams/hour).

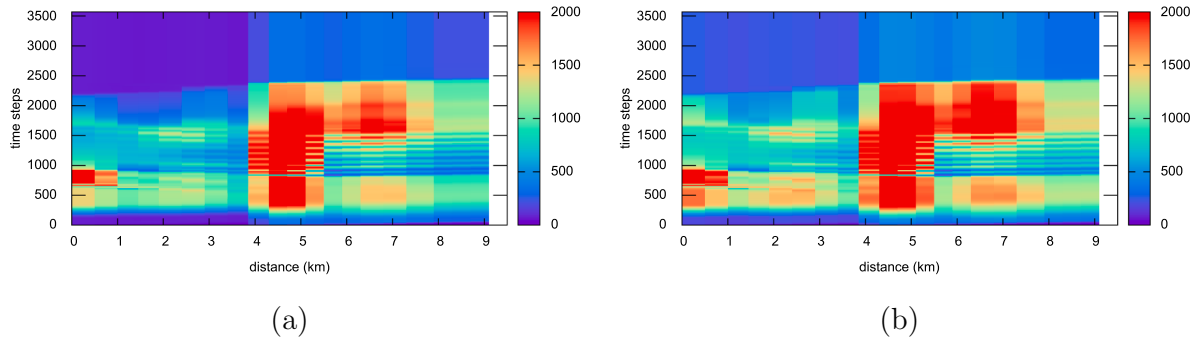


Fig. 13. No-control NO_x emissions (grams/hour) along Route 1 motorway links (grams/hour) due to: (a) Euro3 diesel trucks and (b) total NO_x emissions.

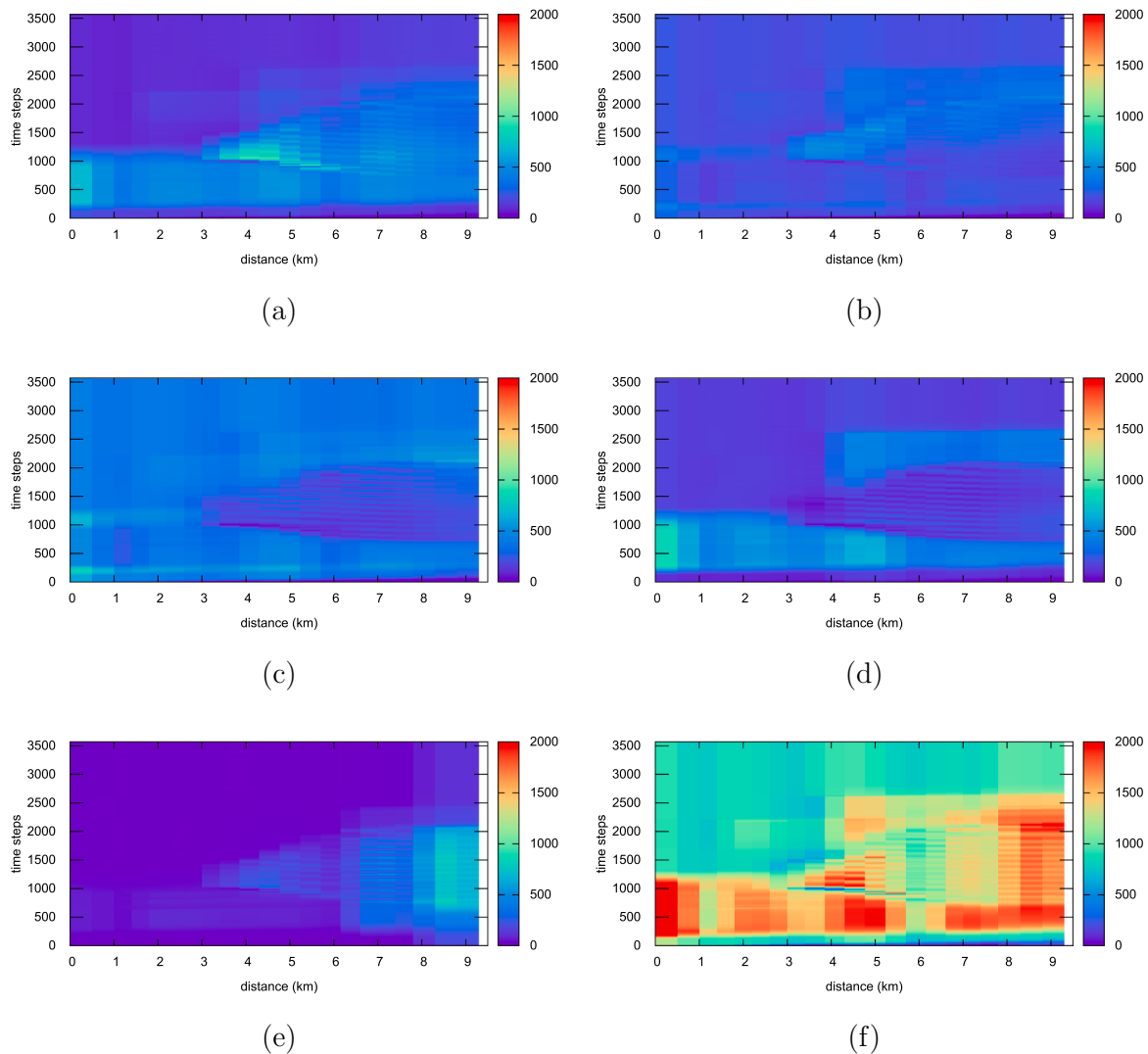


Fig. 14. No-control CO emissions (grams/h) along Route 2 motorway links (grams/hour) due to: (a) Euro1 pc, (b) Euro2 pc, (c) Euro3 pc, (d) Euro4 pc, (e) Euro3 diesel trucks and (f) total CO emissions.

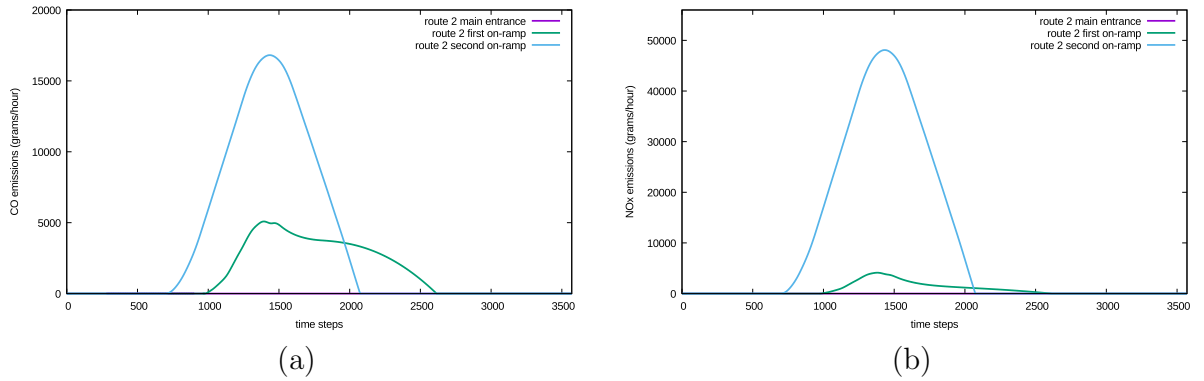


Fig. 15. No-control Route 2 total emissions at on-ramps. (a) CO (grams/hour), (b) NOx (grams/hour).

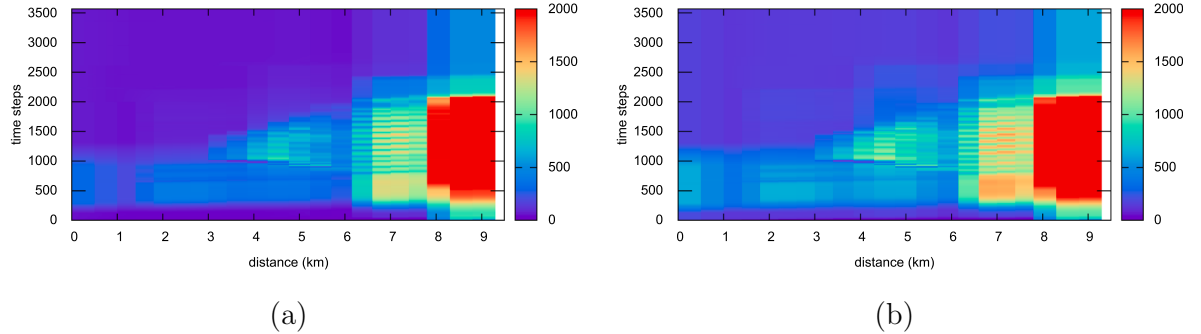


Fig. 16. No-control NOx emissions (grams/hour) along Route 2 motorway links (grams/hour) due to: (a) Euro3 diesel trucks and (b) total NOx emissions.

Table 3

Downstream distance (km) in the motorway from the origin for calculating the equity index.

	Main entrance	First on-ramp	Second on-ramp
Route 1	1.9	2.0	1.6
Route 2	1.8	2.3	1.5

Table 4

Case study scenarios parameters.

Scenario	ω_0	ω_1	ω_2	ω_3	ω_4	ω_5	$\omega_{z,term}$	w_{max} (veh)	
								(main entrances)	(on-ramps)
1	1.0	0.0	0.0	1E-3	0.0	0.0	0.0	$+\infty$	$+\infty$
2	0.0	0.0	0.0	1E-3	3E-3	0.0	0.0	$+\infty$	$+\infty$
3	0.0	0.0	0.0	1E-3	0.0	1E-7	1E-5	$+\infty$	$+\infty$
4	0.0	0.0	0.0	1E-3	3E-3	1E-7	1E-5	$+\infty$	$+\infty$
5	1.0	100.0	1E-5	1E-3	3E-3	1E-7	1E-5	400	100
6	1.0	100.0	1E-5	1E-3	3E-3	0.0	0.0	400	100
7	1.0	100.0	1E-5	1E-3	3E-3	1E-7	1E-5	200	50
8	1.0	100.0	1E-5	1E-3	3E-3	0.0	0.0	200	50

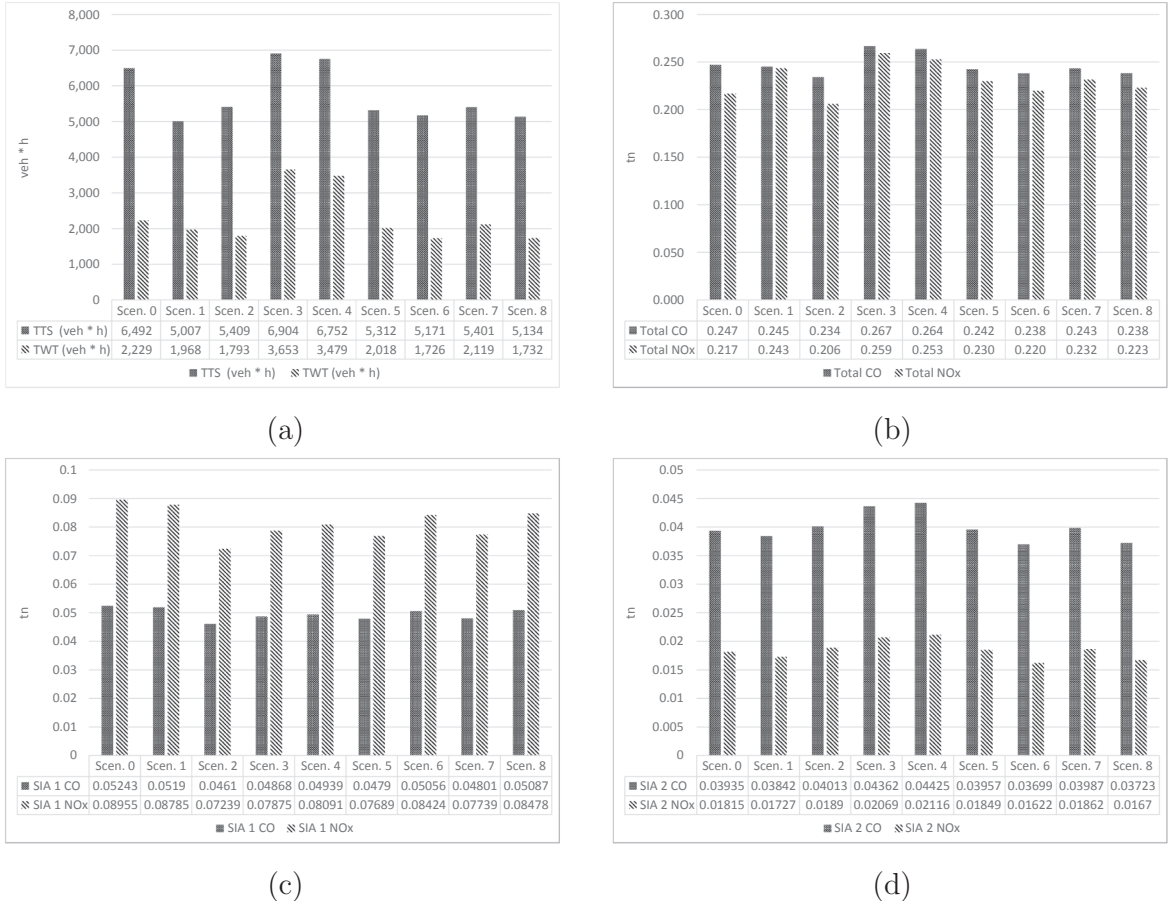


Fig. 17. Scenario average values compared to the no-control case. (a) TTS and TWT (b) total network CO and NO_x emissions (c) SIA 1 CO and NO_x emissions (d) SIA 2 CO and NO_x emissions.

only objective. Scenario 2 is the minimisation of total network emissions only without local SIA emissions constraints and without considering the TTS, equity and queue constraints. Scenario 3 is the same regarding efficiency, equity and maximum queues and in addition the total network emissions are ignored; only the local SIA constraints (60) and (61) are considered. Scenario 4 is the combination of scenarios 2 and 3, i.e. total emissions minimisation and local SIA constraints. Scenario 5 is a full control scenario considering efficiency, equity, maximum queues along with global and local environmental constraints. Scenario 6 is the same as scenario 5, but without the local SIA constraints. The maximum queues are 400 vehicles for the mainstream entrances and 100 vehicles for the on-ramps. Setting these maximum queues to 200 and 50 provides scenarios 7 and 8. Table 4 provides the weighting parameters of (76) and maximum queues for each scenario. $\omega_{z,tot}$ in (74) are all set to 1 and $\omega_{z,term}$ has the same value for all pollutants. The control time step is set to $T_c = 0.0333$ h leading to $a_{cm} = 34$ model time steps.

For each scenario a total of 12 experiments were conducted executing the stochastic search algorithm with a population of 6 individuals and 240 maximum number of iterations. Furthermore, a single run of the algorithm was executed with 9 individuals and 1,300 maximum iterations, referred to as increased iterations runs.

8. Results and discussion

The results from the repeated experiments are summarised in Fig. 17 and the full results for each scenario and their comparison with respect to scenario 0 are included in the accompanying MSExcel file.

The maximum efficiency scenario 1 achieves the best result for the mean TTS reduction with respect to the no-control case with a decrease of 22.87%. Comparing the results of scenario 1 and 2, it can be seen that efficiency and global emissions are partially competing. In fact, the maximum efficiency objective increases the global NO_x emissions and keeps the CO at similar levels as in the no-control case. On the other hand, the minimum global emissions objective does result to a decreased level of TTS serving partially the goal of efficiency. A decrease of 6.18 percentage units on the TTS improvement by scenario 2 compared to scenario 1, results to an improvement of 4.48 percentage units on CO emissions and 17.29 percentage units on NO_x with respect to the improvements achieved by scenario 1. In scenario 2, the reduction of both the TTS and the global NO_x emissions is achieved something which is not true for the

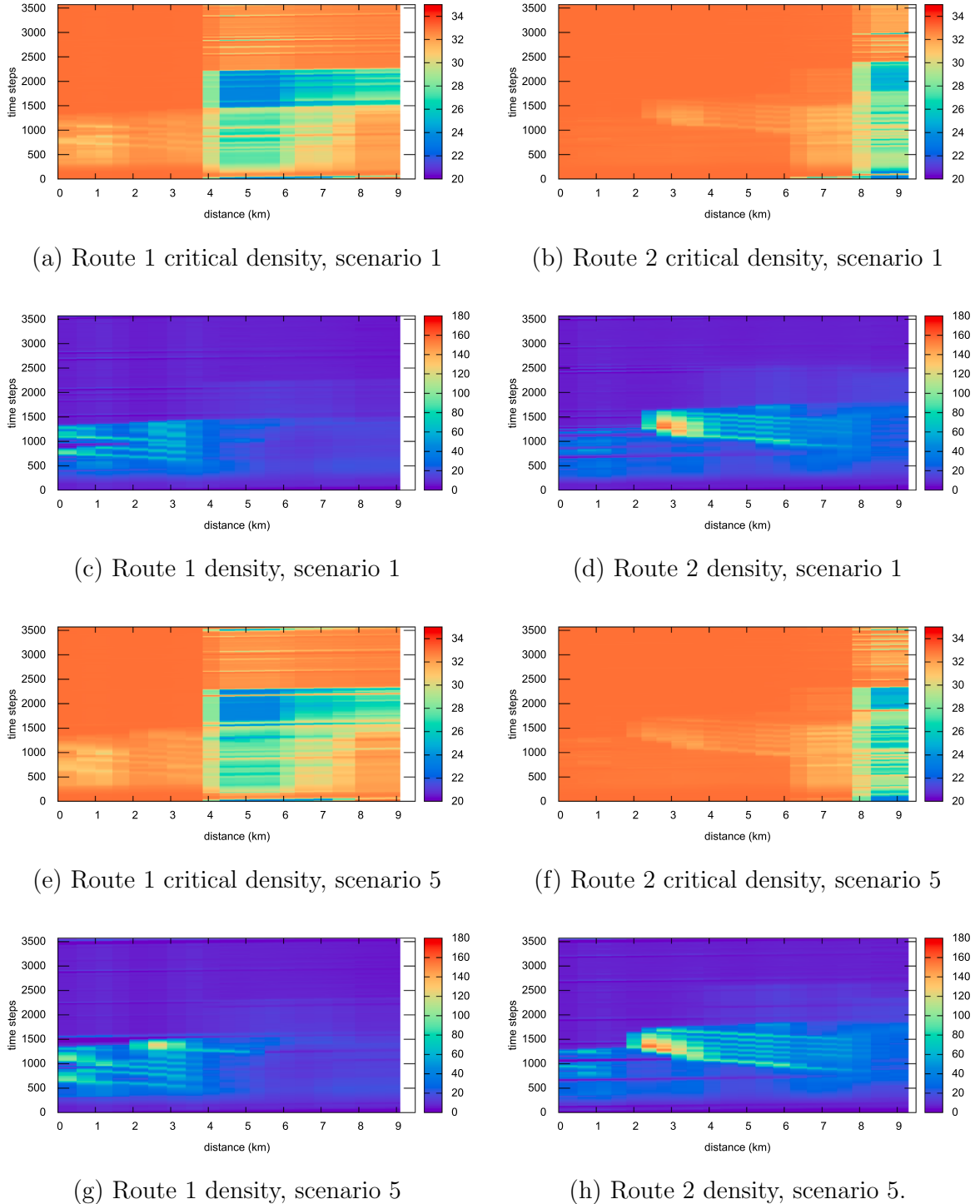


Fig. 18. CRM control profiles of critical density and density based on the increased iterations optimisation algorithm runs of scenarios 1 and 5.

maximum efficiency case scenario 1. Furthermore, the minimum global emissions policy is more equitable from the maximum efficiency, since the mean $\Phi_{equi,tot}$ is 0.37 for scenario 2 and 1.24 for scenario 1.

The reason for this behaviour, is that the most efficient ramp metering actions restrain heavily the traffic entering the network from the on-ramps that are directly upstream (and at a short distance) from the bottleneck, whereas more equitable strategies spread the queues through the maximum queue length constraints mechanism to the upstream on-ramps at further distance away, see (Kotsialos and Papageorgiou, 2004a). With a maximum queue violation weight equal to zero, scenario 1 is impervious to large queues built in the

network, unless the TWT starts having a detrimental effect on the TTS. Similarly, the minimum global emissions policy cannot afford large queues at the on-ramps, since they result to increased emissions at origin links. Hence, the weighted sum of global emissions is a viable alternative as a stand alone cost criterion in the optimal control problem as it is capable on its own of striking a balance between environmental impact, efficiency and equity.

However, the introduction of local environmental policies in the form of constraints (60) and (61) have a detrimental effect on the performance of the global emissions minimisation policy. This is shown in the results of scenario 4. Introducing penalties for local emissions constraint violations leads to traffic profiles worst than in the no-control case, with the exception of the SIA 1 performance indicators. It can be seen from Fig. 17 that in order for the SIA 1 performance indices to be improved, all other indices are compromised. In other words, the introduction of a limited space and time policy of protecting a SIA, severely disrupts the environmental and traffic efficiency performance of a global emissions minimisation policy. Such a myopic policy, which if fully applied in scenario 3, degrades the network wide positive effects of CRM. Scenario 3 is the pure local emissions minimisation policy and in all accounts is much worst than all the other scenarios, including the no-control case, except for SIA 1. SIA 2 is further compromised for the benefit of SIA 1.

SIA 1 and SIA 2 face the reverse problem of local CO and NO_x emissions, as can be seen from Fig. 17 (c) and (d). Because traffic in SIA 1 has a higher proportion of trucks, NO_x emissions are higher than CO, whereas the CO emissions in SIA 2 are much larger than NO_x because traffic consists more of pc than trucks. SIA 1 has a more severe problem than SIA 2 and the solutions of scenario 3 try to strike a balance only between the two local emissions profiles without considering any global environmental or efficiency performance metric. The results of scenario 4 indicate a sensitivity of the global emissions minimisation policy, although this could be attributed to the value of ω_3 , which implicitly assigns larger weight to the local constraints violations compared to the TTS in the objective function of scenarios 5–8. The question of whether the TTS can be replaced by the weighted global emissions requires further investigation, but needs to be examined not only for the CRM problem but for the more general integrated RM, RG and VSL problem.

The results of scenarios 5–8 show a more balanced performance. The CRM is consisted in improving the traffic profile. Compared to the no-control case, the strategy increases the global NO_x emissions, but not the CO. Improvements are observed in the SIA 1 indices for the total mass emitted but not for the emissions rates constraints, particularly for NO_x. The disruptive behaviour of the local environmental policies is still present, but to a lesser degree, since the TTS is now the dominant element in the objective function. However, a competitive relationship between the CO and the NO_x emissions at both the global and the local level is observed. This is to be expected given the variability of traffic composition.

The multi-class model used provides an additional insight on the mechanism a control strategy works. Fig. 18 shows the spatio-temporal profile of the critical density and density from the increased iterations versions of scenario 1 and 5 for Routes 1 and 2. Comparing Figs. 18(a) and (e) with Fig. 10(a), it can be seen that the CRM strategy delays the inflow of trucks into the mainstream. The solid block of low critical density flow between the 4th and the 7th km of Route 1 in the no-control case begins to form at about the 1,000th model time step and is dissolved at about the 1,600th step. The same block in the control case is formed later on in the same area, starting at about the 1,600th step and finishing at around the 2,200th. Afterwards and for the rest of the time horizon, the flow in the control case has a larger proportion of trucks than in the no-control case. It is the temporal translation of the large truck inflow that allows the faster moving pc traffic to exit the system sooner, supporting this way the maximisation of the time weighted outflows, which is equivalent to TTS minimisation. This behaviour leads to the extension of the truck inflow from Route 1 to Route 2 later in the time horizon and as a result the decrease of the critical density at the downstream area of Route 2 as shown in Figs. 18(b) and (f). It is for this reason the congestion pattern of Route 2 that appears in the no-control case in Fig. 9(c) is still present, although with much reduced spread.

Comparing the density and critical density profiles in Fig. 18 of scenarios 1 and 5, the impact of limiting the on-ramp storage capacity can be seen. Congestion is unavoidable in view of the absence of re-routing, because the traffic demand exceeds the network's supply of capacity. The challenge for a TTS minimising CRM strategy is to decide the location, extension and duration of congestion by creating queues at the origin and congestion in the motorway links. The congestion patterns in scenarios 1 and 5 are very similar. The limited storage capacity of scenario 5 creates the need for releasing traffic earlier than in scenario 1 due to the penalisation of queue sizes larger than the maximum desired levels. For Route 1 this results to a slightly heavier congestion in its first 4 km, compared to scenario 1, due to the higher discharge outflow from its main entrance. Congestion, though, is contained within this area and is not allowed to propagate further downstream cancelling this way the main cause of traffic deterioration in Route 1, which is the spillback from Route 2 via MJ2. In Route 2, the storage capacity limitation of scenario 5 results to the spatial extension of congestion upstream up to the point where the connector link from Route 1 joins Route at MJ1, whereas in scenario 1 this congestion extends further downstream, protecting effectively Route 1 from spillback via MJ1.

Another interesting result can be seen in the critical density profiles of Fig. 18, where areas of faster moving traffic with higher critical density are “cutting through” areas with lower critical density. This is shown more pronouncedly in Fig. 18(e). Scenario 5 predicts traffic with high pc composition travelling in Route 1 reflecting the increase of the mean speed due to the presence of fewer trucks in the traffic stream. Hence, the CRM strategy based on the multi-class model is implicitly affecting and regulating the characteristic features of the traffic flow process, which in the single-class model are considered as fixed.

Compared, with their counterparts (scenarios 5 and 7), scenarios 6 and 8 are more efficient and better at the total network wide emissions at the cost of higher violations of the SIA constraints (60) and (61) with the exception of the SIA 2 constraints (61). Interestingly, the activation of the (61) constraints increases the rate of emissions at SIA 2.

With respect to scenarios 6 and 8, the TTS is reduced by 20.35% and 20.92%, respectively. Both include explicitly the TTS and the total emissions in their objective function but they are not restrained from SIA constraints (60) and (61). Scenario 6 is slightly less efficient on average from scenario 8 despite the fact that more storage capacity is available in it than in 8. Fig. 19 provides the density

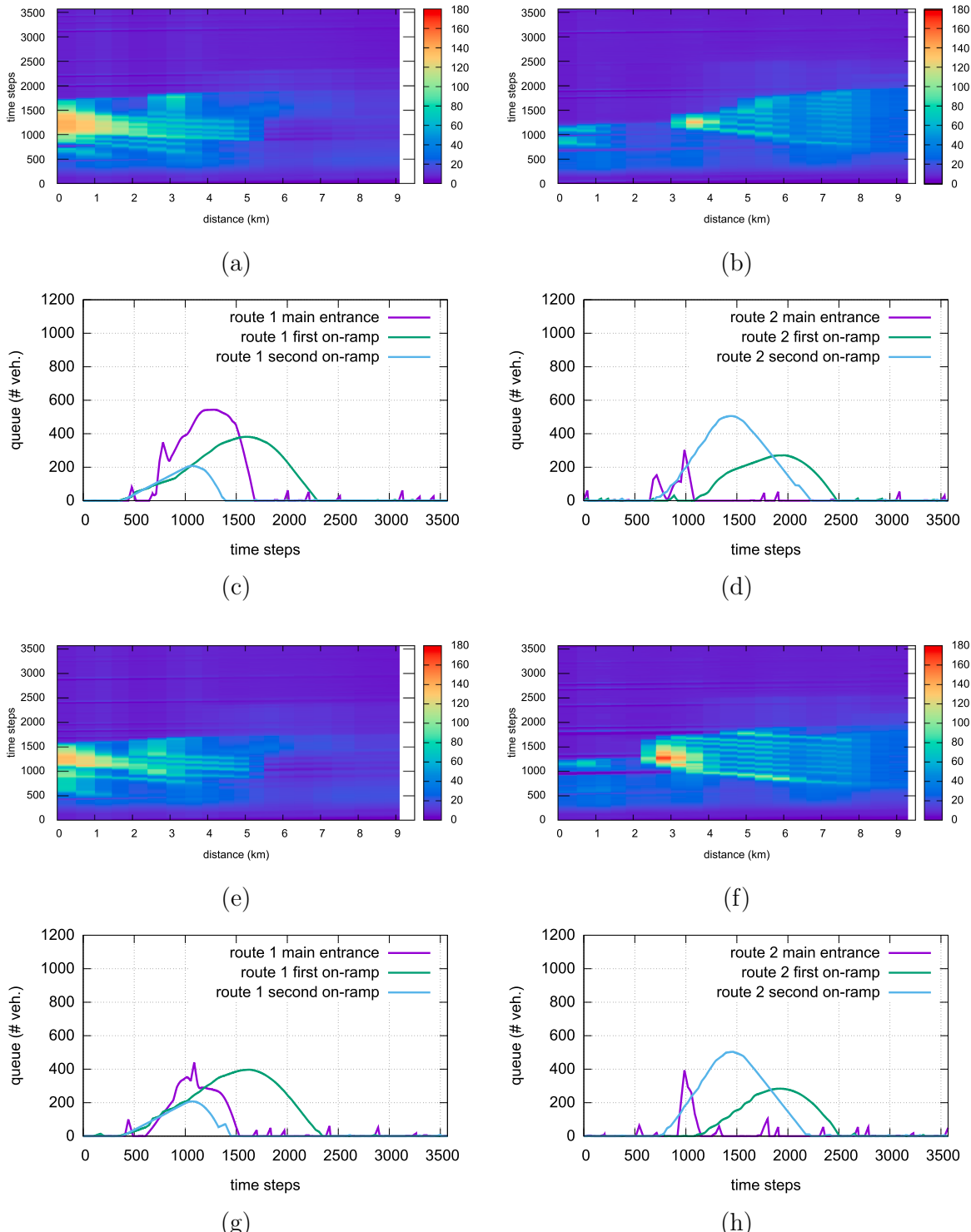


Fig. 19. Scenario 6 profiles: (a) Route 1 density. (b) Route 2 density. (c) Route 1 queues. (d) Route 2 queues. Scenario 8 profiles: (e) Route 1 density. (f) Route 2 density. (g) Route 1 queues. (h) Route 2 queues.

and queue profiles along the two routes, based on the increased iterations algorithm runs. The solution of scenario 6 favours the improvement of traffic conditions in Route 2 at the expense of Route 1. The key parameter is the size of the queues formed in the main entrances. The pressure for smaller queue sizes in scenario 8 results to the reduction of the main entrance queue of Route 1 at the expense of the traffic conditions of Route 2, where a wider congestion appears and a larger queue is built at the main entrance, compared to the solution of scenario 6. The overall result, however, is marginally better in scenario 8 than in 6. Essentially, Fig. 19(a)-(d) shows the results of converging to a good local minimum, since the solution of scenario 8 is within the search space of scenario 6. The algorithm's convergence and its association to the available storage capacity should be further investigated in order to identify the proper exploration/exploitation balance of the DE search.

The previous discussion focused on the open-loop optimal control problem solutions over the entire simulation horizon of 3.5 h or 3,571 steps. It took the DE algorithm about 22.5 min to complete 240 iterations using a population of 6 individuals on a linux based laptop with i3 dual core Pentium at 2.40 GHz and 4 GB of RAM. DE itself has a very good performance, since for a $630 (= 6 \times [3, 571 / 34])$ dimensional static optimisation problem, it converges to good quality solutions using a very small population. Rolling horizon MPC implementations do not require long prediction time horizons. In Kotsialos et al. (2005) rolling horizon investigations are reported for the AMOC tool, applied on a larger network than the one considered here, with prediction horizon of 1 h and application horizon of 10 min. Because AMOC utilises gradient-based optimisation and uses a single-class model, it requires only a few seconds for converging to an optimal open-loop solution to the CRM problem. Clearly, the DE convergence is several times the order of scale of AMOC's. However, since the convergence properties of DE have not been investigated it may turn out that good results are obtained with fewer iterations for smaller horizon problems. The detailed investigation of DE's convergence properties will be reported elsewhere. Such an investigation involves studying the rolling horizon MPC hierarchical structure described in (Kotsialos et al., 2005) for different combinations of prediction and application time horizons. The possibility of using local controllers is an open option as well, see (Kotsialos et al., 2005a; Papamichail et al., 2010).

9. Conclusions and future work

This paper has presented a new multi-class macroscopic second-order traffic flow model and an optimal control problem formulation for CRM with global and local environmental objectives. This problem formulation is capable of meeting the requirements of complex environmental policies regarding hot gas emissions at the global and local levels. The enabling element behind the proposed framework is the multi-class model developed, which is an extension of the well-known single-class METANET model.

The modelling approach followed is different from similar efforts reported in the literature in the sense that the traffic flow is not split into virtual traffic streams, one for each vehicle class, but instead a single traffic stream is considered, just as in the single-class case. The difference is that the traffic parameters are treated as varying over time along with traffic composition and density. The model parameters of the fundamental diagram, the mean speed and queue equations change depending on the composition of pc and trucks at any given point in time. The functional dependence of these relationships is based on sigmoid surfaces. This approach has the benefit of using one extra dynamic equation per vehicle class instead of using two and allows the grouping of vehicle classes with different environmental parameters but similar traffic behaviour into general classes.

The model used for estimating the hot gas emissions is the COPERT model, which provides emission factors for a very broad range of vehicle classes and pollutants using the mean speed as the main input. The analysis and the case study presented here considered two pollutants, CO and NO_x , four pc classes and a single truck class. Extending the model into more pc classes, truck classes and pollutants is straightforward.

This multi-class model was used for designing a CRM strategy as an optimal control problem. A stochastic search algorithm was used for solving the static problem and a number of scenarios were visited. The results indicate that the approach followed is sound and CRM strategies can be designed having as their goal increased network efficiency, improved equity and reduced environmental impact. A new element introduced by multi-class based CRM is the fact that the controller through the class-related information available is allowed to manage the features characterising the traffic flow, in terms of critical density, free flow speed, relaxation and anticipation. This kind of management is realised implicitly by regulating the on-ramps' outflows and their composition. More investigations are required for mapping out this mechanism.

Future work needs to be conducted for the validation of the multi-class model based on real data collected from the field. Calibration of the model parameters to fit empirical data is necessary for obtaining a model representing reality with sufficient accuracy. Modern traffic flow sensors and devices provide categorization data based on vehicle length, but not information about engine technology and truck load. A model validation process based on both traffic and environmental sensor data is necessary.

The model presented assumes instant change of the fundamental diagram and speed equation parameters to changing composition and density. This implies the relaxation and anticipation processes are changing with the same rate. More attention may be required for this issue. An interesting direction of future research is the introduction of equations modelling slower dynamics for these parameters, leading to higher order models.

In the model developed here, the turning rates used are applied at the cross-class flow. However, class-specific turning rates can be introduced into the model for representing more realistically the routing behaviour of the different vehicle classes. Extending further this reasoning, a destination oriented multi-class model can also be developed. Such a model would allow the development of model-based route guidance control and the integration of ramp metering and route guidance into a single controller structure. Further integrating variable speed limits in the control structure is another important direction of work.

A question related to the design of MPC is the relevance of the cost criterion used. The relationship between the TTS and the weighted total emissions of all pollutants and how they should be employed for obtaining relevant solutions needs to be investigated in

detail not only for the CRM but for the integrated control problem as well.

In the investigations presented here, the parameters of the local environmental constraints were kept constant throughout the time horizon. However, restrictions can be progressive and their effect should be investigated when they vary over time.

An interesting area for further research relates to investigating the strategy's performance in a rolling horizon framework. In the application presented in Section 7, the problem dimension is quite large since its scope is the whole time horizon of 3.5 h. The stochastic search algorithm used here for solving the optimal control problem required significant computation time to converge to solutions of sufficient quality. It is interesting to investigate if its convergence properties are sufficient for smaller horizon problems that would be implemented in a rolling horizon fashion. Another issue requiring investigation for a rolling horizon application is the impact of errors in the class-oriented demand predictions and initial state estimations.

Finally, the development of a gradient based optimisation algorithm for solving the optimal control problem is an important direction of work. This work can be combined with a broader effort of evaluating the convergence performance of other population based algorithms, apart from Differential Evolution.

Acknowledgement

The views and opinions expressed in this paper are personal and do not reflect the views and opinions of the Public Power Corporation – Hellas S.A.

Appendix A. Supplementary material

Supplementary data associated with this article can be found, in the online version, at <https://doi.org/10.1016/j.trc.2021.103106>.

References

- Ahn, K., 1998. Microscopic fuel consumption and emission modeling. PhD thesis, Virginia Tech.
- Aw, A., Rascle, M., 2000. Resurrection of "second order" models of traffic flow. *SIAM J. Appl. Mathe.* 60 (3), 916–938.
- Bagnerini, P., Rascle, M., 2003. A multiclass homogenized hyperbolic model of traffic flow. *SIAM J. Mathe. Anal.* 35 (4), 949–973.
- Balzotti, C., Briani, M., de Filippo, B., Piccoli, B., 2019. Evaluation of no x emissions and ozone production due to vehicular traffic via second-order models. arXiv preprint arXiv:1912.05956.
- Bellomo, N., Dogbe, C., 2011. On the modeling of traffic and crowds: A survey of models, speculations, and perspectives. *SIAM Rev.* 53 (3), 409–463.
- Caligaris, C., Sacone, S., Siri, S., 2007. Optimal ramp metering and variable speed signs for multiclass freeway traffic. In: 2007 European Control Conference (ECC). IEEE, pp. 1780–1785.
- Caligaris, C., Sacone, S., Siri, S., 2010. On the Payne-Whitham differential model: stability constraints in one-class and two-class cases. *Appl. Mathe. Sci.* 4 (76), 3795–3821.
- Chakraborty, U.K. (Ed.), 2008. Advances in Differential Evolution, volume 143 of Studies in Computational Intelligence. Springer.
- Chanut, S., Buisson, C., 2003. Macroscopic model and its numerical solution for two-flow mixed traffic with different speeds and lengths. *Transport. Res. Rec.* 1852 (1), 209–219.
- Chen, J., Yu, Y., Guo, Q., 2019. Freeway traffic congestion reduction and environment regulation via model predictive control. *Algorithms* 12 (10), 220.
- Coifman, B., 2015. Empirical flow-density and speed-spacing relationships: Evidence of vehicle length dependency. *Transport. Res. Part B: Methodol.* 78, 54–65.
- Cruz, L., 2002. Efficient evolutionary algorithms for optimal control. PhD thesis, Wageningen University, The Netherlands.
- Csikós, A., Varga, I., Hangos, K.M., 2015. Modeling of the dispersion of motorway traffic emission for control purposes. *Transport. Res. Part C: Emerg. Technol.* 58, 598–616.
- Csikós, A., Varga, I., Hangos, K.M., 2018. A hybrid model predictive control for traffic flow stabilization and pollution reduction of freeways. *Transport. Res. Part D: Transport Environ.* 59, 174–191.
- Delle Monache, M.L., Chi, K., Chen, Y., Goatin, P., Han, K., Qiu, J.-M., Piccoli, B., 2018. A three-phase fundamental diagram from three-dimensional traffic data. Technical Report 01864628, HAL.
- Deo, P., de Schutter, B., Hegyi, A., 2009. Model predictive control for multi-class traffic flows. *IFAC Proc. Vol.* 42 (15), 25–30.
- Dynamic Systems and Simulation Laboratory, 2008. Technical University of Crete, Chania, Crete, Greece. METANET Documentation.
- Ferrara, A., Pasquale, C., Sacone, S., Siri, S., 2017. Congestion and emissions reduction in freeway traffic networks via supervisory event-triggered control. *IFAC-PapersOnLine*, 50(1), 4240–4245, 20th IFAC World Congress.
- Fleming, P.J., Purshouse, R.C., 2002. Evolutionary algorithms in control systems engineering: a survey. *Control Eng. Practice* 10 (11), 1223–1241.
- Hall, F.L., 1996. Traffic stream characteristics. *Traffic Flow Theory*. US Federal Highway Administration, 36.
- Helbing, D., Treiber, M., 2002. Critical discussion of synchronized flow. Cooper@tive Tr@nsport Dyn@ ics, 1(2.12):24. (Internet Journal, www.TrafficForum.org/journal).
- Kotsialos, A., 2014. Nonlinear optimisation using directional step lengths based on RPROP. *Optim. Lett.* 8 (4), 1401–1415.
- Kotsialos, A., 2019. Constrained nonlinear optimisation using resilient backpropagation as search method. In: 8th Intern. Symposium and 30th National Conference on Operational Research. Hellenic Operation Research Society, pp. 81–84.
- Kotsialos, A., 2020. A second order multi-class macroscopic traffic flow model with time varying parameters for environmentally sustainable coordinated ramp metering control. In: Proc. of the XIV Balkan Conference on Operational Research (Virtual BALCOR 2020), Thessaloniki, Greece.
- Kotsialos, A., Papageorgiou, M., 2001. The importance of traffic flow modeling for motorway traffic control. *Networks Spatial Econ.* 1 (1–2), 179–203.
- Kotsialos, A., Papageorgiou, M., 2004a. Efficiency and equity properties of freeway network-wide ramp metering with amoc. *Transport. Res. Part C: Emerg. Technol.* 12 (6), 401–420.
- Kotsialos, A., Papageorgiou, M., 2004b. Motorway network traffic control systems. *Eur. J. Oper. Res.* 152 (2), 321–333.
- Kotsialos, A., Papageorgiou, M., 2004c. Nonlinear optimal control applied to coordinated ramp metering. *IEEE Trans. Control Syst. Technol.* 12 (6), 920–933.
- Kotsialos, A., Papageorgiou, M., Diakaki, C., Pavlis, Y., Middelham, F., 2002a. Traffic flow modeling of large-scale motorway networks using the macroscopic modeling tool METANET. *IEEE Trans. Intell. Transp. Syst.* 3 (4), 282–292.
- Kotsialos, A., Papageorgiou, M., Mangeas, M., Hadj-Salem, H., 2002b. Coordinated and integrated control of motorway networks via non-linear optimal control. *Transport. Res. Part C: Emerg. Technol.* 10 (1), 65–84.
- Kotsialos, A., Papageorgiou, M., Middelham, F., 2005. Local and optimal coordinated ramp metering for freeway networks. *J. Intell. Transport. Syst.* 9 (4), 187–203.

- Kotsialos, A., Papageorgiou, M., Hayden, J., Higginson, R., McCabe, K., Rayman, N., 2006. Discrete release rate impact on ramp metering performance. *IEE Proc.-Intell. Transport Syst.* 153 (1), 85–96.
- Ligerink, N.E., de Lange, R., Schoen, E., 2009. Refined vehicle and driving-behaviour dependencies in the VERSIT+ emission model. In: ETAPP Symposium.
- Lin, X., Immers, B., Viti, F., Tampère, C., 2012. Evaluating the impact of environmental constraints in networks: formulation and analysis in a simple case. In: Gebhard Wulffhorst and Benjamin Büttner, editors, *Transportation Demand Management: Insights from the mobil.TUM 2012 International Scientific Conference on Mobility and Transport*. Technical University of Munich, Germany.
- Lin, X., Tampère, C., Viti, F., Immers, B., 2016. The cost of environmental constraints in traffic networks: assessing the loss of optimality. *Networks Spatial Econ.* 16 (1), 349–369.
- Liu, S., de Schutter, B., Hellendoorn, H., 2014a. Model predictive traffic control based on a new multi-class METANET model. *IFAC Proc.* Vol. 47 (3), 8781–8786.
- Liu, S., de Schutter, B., Hellendoorn, H., 2014b. Model predictive traffic control based on a new multi-class METANET model. *IFAC Proc.* Vol. 47 (3), 8781–8786, 19th IFAC World Congress.
- Liu, S., Sadowska, A., Frejo, J.R.D., Núñez, A., Camacho, E.F., Hellendoorn, H., de Schutter, B., 2016. Robust receding horizon parameterized control for multi-class freeway networks: A tractable scenario-based approach. *Int. J. Robust Nonlinear Control* 26 (6), 1211–1245.
- Liu, S., Hellendoorn, H., de Schutter, B., 2017. Model predictive control for freeway networks based on multi-class traffic flow and emission models. *IEEE Trans. Intell. Transp. Syst.* 18 (2), 306–320.
- Logghe, S., Immers, L.H., 2008. Multi-class kinematic wave theory of traffic flow. *Transport. Res. Part B: Methodol.* 42 (6), 523–541.
- Luo, L., Ge, Y.-E., Zhang, F., Ban, X.J., 2016. Real-time route diversion control in a model predictive control framework with multiple objectives: Traffic efficiency, emission reduction and fuel economy. *Transport. Res. Part D: Transport Environ.* 48, 332–356.
- Méndez, A.R., Marques, W., Velasco, R.M., 2019. Multi-class fundamental diagrams from the Prigogine–Herman–Boltzmann equation. *Phys. Scr.* 94 (11), 115008.
- Ngoduy, D., 2010. Multiclass first-order modelling of traffic networks using discontinuous flow-density relationships. *Transportmetrica* 6 (2), 121–141.
- Ngoduy, D., 2011. Multiclass first-order traffic model using stochastic fundamental diagrams. *Transportmetrica* 7 (2), 111–125.
- Ntziachristos, L., Kouridis, C., 2007. Road transport emission chapter of the EMEP/CORINAIR Emission Inventory Guidebook. Technical report, European Environment Agency. Technical Report No. 16/2007, Copenhagen, Denmark.
- Othman, B., de Nunzio, G., di Domenico, D., Canudas-de Wit, C., 2019. Ecological traffic management: A review of the modeling and control strategies for improving environmental sustainability of road transportation. *Ann. Rev. Control* 48, 292–311.
- Papageorgiou, M., 1990. Dynamic modeling, assignment, and route guidance in traffic networks. *Transport. Res. Part B: Methodol.* 24 (6), 471–495.
- Papageorgiou, M., Kotsialos, A., 2002. Freeway ramp metering: An overview. *IEEE Trans. Intell. Transp. Syst.* 3 (4), 271–281.
- Papageorgiou, M., Hadj-Salem, H., Blosseville, J.-M., 1991. Alinea: A local feedback control law for on-ramp metering. *Transp. Res. Rec.* 1320 (1), 58–67.
- Papageorgiou, M., Diakaki, C., Dinopoulou, V., Kotsialos, A., Yibing, W., 2003. Review of road traffic control strategies. *Proc. IEEE* 91 (12), 2043–2067.
- Papamichail, I., Kotsialos, A., Margonis, I., Papageorgiou, M., 2010a. Coordinated ramp metering for freeway networks – A model-predictive hierarchical control approach. *Transport. Res. Part C: Emerg. Technol.* 18 (3), 311–331.
- Papamichail, I., Papageorgiou, M., Vong, V., Gaffney, J., 2010b. Heuristic ramp-metering coordination strategy implemented at Monash freeway, Australia. *Transport. Res. Rec.* 2178 (1), 10–20.
- Pasquale, C., Sacone, S., Siri, S., 2014. Ramp metering control for two vehicle classes to reduce traffic emissions in freeway systems. In: 2014 European Control Conference (ECC), pp. 2588–2593.
- Pasquale, C., Liu, S., Siri, S., Sacone, S., de Schutter, B., 2015a. A new emission model including on-ramps for two-class freeway traffic control. In: 2015 IEEE 18th International Conference on Intelligent Transportation Systems, pp. 1143–1149.
- Pasquale, C., Papamichail, I., Roncoli, C., Sacone, S., Siri, S., Papageorgiou, M., 2015b. A nonlinear optimal control approach for two-class freeway traffic regulation to reduce congestion and emissions. In: 2015 European Control Conference (ECC), pp. 2646–2651.
- Pasquale, C., Anghinolfi, D., Sacone, S., Siri, S., Papageorgiou, M., 2016a. A comparative analysis of solution algorithms for nonlinear freeway traffic control problems. In: 2016 IEEE 19th International Conference on Intelligent Transportation Systems (ITSC), pp. 1773–1778.
- Pasquale, C., Anghinolfi, D., Sacone, S., Siri, S., Papageorgiou, M., 2016b. A two-class traffic control scheme for reducing congestion and improving safety in freeway systems. In: 2016 IEEE 19th International Conference on Intelligent Transportation Systems (ITSC). IEEE, pp. 1767–1772.
- Pasquale, C., Sacone, S., Siri, S., de Schutter, B., 2017a. A multi-class model-based control scheme for reducing congestion and emissions in freeway networks by combining ramp metering and route guidance. *Transport. Res. Part C: Emerg. Technol.* 80, 384–408.
- Pasquale, C., Sacone, S., Siri, S., Ferrara, A., 2017b. Supervisory multi-class event-triggered control for congestion and emissions reduction in freeways. In: 2017 IEEE 20th International Conference on Intelligent Transportation Systems (ITSC), pp. 1–6.
- Pasquale, C., Sacone, S., Siri, S., Ferrara, A., 2018. A multi-class decentralised event-triggered control framework for congestion and emission reduction in freeway networks. In: Proceedings of the 15th IFAC Symposium on Control in Transportation Systems, vol. 51, IFAC PapersOnLine, pp. 291–298.
- Pasquale, C., Sacone, S., Siri, S., Ferrara, A., 2019. Traffic control for freeway networks with sustainability-related objectives: Review and future challenges. *Ann. Rev. Control* 48, 312–324.
- Pasquale, C., Sacone, S., Siri, S., Ferrara, A., 2020. Hierarchical centralized/decentralized event-triggered control of multiclass traffic networks. *IEEE Trans. Control Syst. Technol.*
- Pavlis, Y., Papageorgiou, M., 1999. Simple decentralized feedback strategies for route guidance in traffic networks. *Transport. Sci.* 33 (3), 264–278.
- Persaud, B.N., Hall, F.L., 1989. Catastrophe theory and patterns in 30-second freeway traffic data—implications for incident detection. *Transport. Res. Part A: Policy Practice* 23 (2).
- Poole, A., Kotsialos, A., 2016a. Second order macroscopic traffic flow model validation using automatic differentiation with resilient backpropagation and particle swarm optimisation algorithms. *Transport. Res. Part C: Emerg. Technol.* 71, 356–381.
- Poole, A., Kotsialos, A., 2016b. Swarm intelligence algorithms for macroscopic traffic flow model validation with automatic assignment of fundamental diagrams. *Appl. Soft Comput.* 38, 134–150.
- Poole, A., Kotsialos, A., 2018. METANET validation of the large-scale Manchester ring-road network using gradient-based and particle swarm optimization. *IEEE Trans. Intell. Transp. Syst.* 19 (7), 2055–2065.
- Qian, Z.S., Li, J., Li, X., Zhang, M., Wang, H., 2017. Modeling heterogeneous traffic flow: A pragmatic approach. *Transport. Res. Part B: Methodol.* 99, 183–204.
- Qin, A.K., Huang, V.L., Suganthan, P.N., 2009. Differential evolution algorithm with strategy adaptation for global numerical optimization. *IEEE Trans. Evol. Comput.* 13 (2), 398–417.
- Riedmiller, M., Braun, H., 1993. A direct adaptive method for faster backpropagation learning: The rprop algorithm. In: IEEE International Conference on Neural Networks. IEEE, pp. 586–591.
- Schnetzler, B., Louis, X., 2013. Anisotropic second-order models and associated fundamental diagrams. *Transport. Res. Part C: Emerg. Technol.* 27, 131–139.
- Schreiter, T., van Lint, H., Hoogendoorn, S.P., 2011. Multi-class ramp metering: Concepts and initial results. In: 2011 14th International IEEE Conference on Intelligent Transportation Systems (ITSC). IEEE, pp. 885–889.
- Schreiter, T., van Wageningen-Kessels, F., Yuan, Y., van Lint, J.W.C., Hoogendoorn, S.P., 2012. Fastlane: Traffic flow modeling and multi-class dynamic traffic management. Technical report, TRAIL Research School, Delft University, The Netherlands.
- Shaikh, P.W., El-Abd, M., Khanafar, M., Gao, K., 2020. A review on swarm intelligence and evolutionary algorithms for solving the traffic signal control problem. *IEEE Trans. Intell. Transp. Syst.* 1–16.
- Smit, R., Smokers, R., Rabé, E., 2007. A new modelling approach for road traffic emissions: VERSIT+. *Transport. Res. Part D: Transport Environ.* 12 (6), 414–422.

- Storn, R., Price, K., 1997. Differential evolution—a simple and efficient heuristic for global optimization over continuous spaces. *J. Global Optim.* 11 (4), 341–359.
- Transportation Research Board, 2000. Washington, DC, USA. Highway capacity manual.
- Treiber, M., Helbing, D., 1999. Macroscopic simulation of widely scattered synchronized traffic states. *J. Phys. A: Math. Gen.* 32 (1), L17.
- Tuerprasert, K., Aswakul, C., 2010. Multiclass cell transmission model for heterogeneous mobility in general topology of road network. *J. Intell. Transport. Syst.* 14 (2), 68–82.
- van Lint, H., Hoogendoorn, S.P., Schreuder, M., 2009. Multi-class first order traffic flow modeling. In: *Traffic and Granular Flow'07*. Springer, pp. 421–426.
- van Wageningen-Kessels, F., 2013. Multi-class continuum traffic flow models: Analysis and simulation methods. Delft University of Technology.
- van Wageningen-Kessels, F., van Lint, H., Hoogendoorn, S.P., Vuik, K., 2014. New generic multiclass kinematic wave traffic flow model: Model development and analysis of its properties. *Transp. Res.* 2422 (1), 50–60.
- Vissol-Gaudin, E., Kotsialos, A., Massey, M.K., Groves, C., Pearson, C., Zeze, D.A., Petty, M.C., 2017. Solving binary classification problems with carbon nanotube/liquid crystal composites and evolutionary algorithms. In: *2017 IEEE Congress on Evolutionary Computation (CEC)*, pp. 1924–1931.
- Wang, Y., Papageorgiou, M., Gaffney, J., Papamichail, I., Guo, J., 2010. Local ramp metering in the presence of random-location bottlenecks downstream of a metered on-ramp. In: *13th International IEEE Conference on Intelligent Transportation Systems*. IEEE, pp. 1462–1467.
- Wang, Y., Kosmatopoulos, E.B., Papageorgiou, M., Papamichail, I., 2014. Local ramp metering in the presence of a distant downstream bottleneck: Theoretical analysis and simulation study. *IEEE Trans. Intell. Transp. Syst.* 15 (5), 2024–2039.
- Wong, G.C.K., Wong, S.C., 2002. A multi-class traffic flow model—an extension of lwr model with heterogeneous drivers. *Transport. Res. Part A: Policy Practice* 36 (9), 827–841.
- Zegeye, S.K., de Schutter, B., Hellendoorn, H., Breunesse, E.A., Hegyi, A., 2013. Integrated macroscopic traffic flow, emission, and fuel consumption model for control purposes. *Transport. Res. Part C: Emerg. Technol.* 31, 158–171.
- Zhang, H.M., 2002. A non-equilibrium traffic model devoid of gas-like behavior. *Transport. Res. Part B: Methodol.* 36 (3), 275–290.